Memoirs of the School of Engineering, Nagoya University
Vol.45, No.2 (1993)

DIFFUSION OF TURBULENT PLUME AROUND A SPHERE

Ikuo NAKAMURA, Yasuhiko SAKAI, Hiroyuki TSUNODA*
and Shengjian LIU**

Department of Mechano-Informatics and Systems

(Received November 15, 1993)

Abstract

In this research, we investigated the influences of the distortion of the flow generated by a sphere on the behaviors of velocity turbulence and plume diffusion. The incident turbulent flow was created by a biplainer square grid, so that the turbulence intensity decays downstream but the velocity field can be recognized roughly isotropic in the upstream region of the sphere. The diffusion field is an axisymmetric point-source plume which develops in this decaying grid turbulence and runs against the sphere frontally.

Before giving the concrete experimental results and discussions, a general explanation on the effect of an obstacle on the turbulent diffusion is provided and the scientific significance of this research is clarified. In the second chapter, after an account of experimental instruments, the details of the conventional statistics of velocity and concentration field are provided. Special concerns are given to the variations of the velocity and concentration fluctuation intensity near the stagnation point. It is shown that the balance equations of velocity and concentration fluctuation intensity are very useful to understand these phenomena. In the third chapter, discussed are mainly the radial distributions of conventional and conditional statistics of concentration field around the sphere and the variation of the concentration detecting frequency along the stagnation line. The data are summarized by imaging a striation structure of a diffusing plume. The final chapter gives a detailed examination of the fractal feature of sets of iso concentration points taken from data on the stagnation line.

* Department of Mechanical System Engineering, Yamanashi University
** Research & Development Division, ULVAC JAPAN, Ltd.

Contents

1. General Introduction

1. 1 The aim of this research

The problem of turbulent diffusion firstly developed by Taylor[1-1)] has two facets, the one is related to the informational aspect that is to determine the transfer probability of fluid particles[1-2)] and the other is concerning to the real world that is pollution in our environment[1-3)], various chemical reactions such as burning, effective mixing and so on. Of course these two facets are intimately related with each other from the viewpoint of fluid mechanics. Since the importance of both theoretical and practical sides, the turbulent diffusion has attracted many research workers. Historical review of it is given in Monin and Yaglom's book[1-2)] and also the works of Sakai[1-4)], Tsunoda[1-5)] and Liu[1-6)] may be useful.

Environmental situation is complex then very many conditions affect turbulent diffusion significantly, the one of which is the geometrical shape over which diffusion proceeds. Buildings[1-3),1-7)], hills[1-7)~1-9)] in the atmosphere and various structures in the ocean[1-3),1-10)] have strong effect of pollutant diffusion. Most prominent effect of these situation can be studied in the case of turbulent diffusion around a simple body, for example cylinder, sphere, cube and so on.

In general, an obstacle causes three kinds of phenomena affecting turbulent diffusion, these are;

(1) flow separation from the body[1-5),1-11)],
(2) distortion of flow field by the body[1-5),1-12),1-13)],
(3) effect of the wall surface of the body[1-3),1-5),1-8)].

Group of the first are increase of turbulence intensity through the instability of separated shear layer, recirculation of mean flow, meandering of diffusion cloud by Karman vortex[1-5),1-9),1-11),1-14)] and down wash induced by reattachment[1-9),1-14)]. The second means not only the rapid spreading of cloud by the obstacle but also changed turbulent field by distortion appreciably affects the diffusion[1-5),1-12),1-13),1-15)~1-23)]. The most important effect of the third comes from the appearance of the stagnation point[1-5),1-13)] which is referred as stagnation point effect in what follows. Examples are diffusing cloud flapping induced by the fluctuation of stagnation point position[1-24)] and striation effect[1-20),1-21)] (see also chapter 3).

In Figure 1.1, the regions where these three effects appear in the flow field around a body are depicted schematically. The effect of the flow separation is observable in the rear region of the body, but the effect of flow distortion is evident mainly in somewhat far region from the body in front of the separation and final wall effect is naturally strong in the very near wall region. Note these three effects have overlap region then to separate each effect completely is usually impossible. Many researches have been reported on the effect of separation, for example, diffusion around cylinder[1-5),1-11),1-25)], disc[1-26),1-27)], cube[1-28),1-29)] and hill[1-8),1-30)] were studied.

In this research, our aim is to investigate the interaction between a non-buoyant plume in the grid-turbulence and a sphere, typical three-dimensional body.

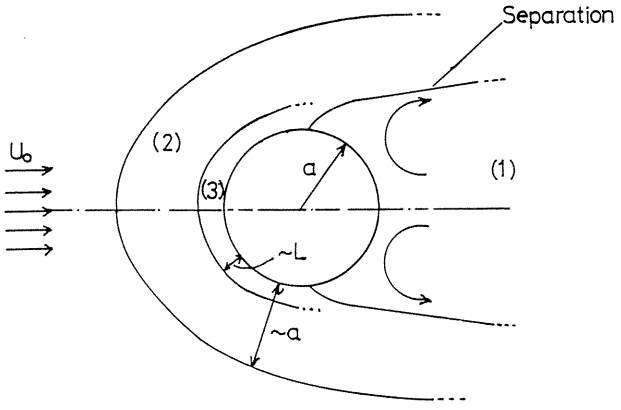

Fig. 1.1 Sketch of the flow field around a body.

1. 2 The influence of flow distortion produced by an obstacle on the material diffusion

Since diffusion process is controlled by the turbulent structure, we summarize at first the effect of flow distortion on the turbulence. This problem appeared in the history of fluid mechanics as how to reduce the turbulent intensity in a wind tunnel and Prandtl pioneered to solve this problem[1-31)]. Afterwards Taylor[1-32)] and also Batchelor & Proudman[1-15)] analyzed the same flow situation. Townsend[1-33)], Tucker[1-34)] examined this problem experimentally. The concept of rapid distortion is a key to solve this problem and the fundamental assumption of the rapid distortion theory is that when the mean flow changes so quickly one can

neglect every non-linear interaction between turbulent eddies and the action of viscosity while the distortion occurs[1-16),1-18)].

The assumption is valid under the following conditions;

$$T_s \sim L_s/U_0 \leq T_u \sim T_\varepsilon \sim L/u' \tag{1.1}$$

$$Re = U_0 L_s/\nu \gg 1\,, \quad Re_\lambda = u'L/\nu \gg 1 \tag{1.2}$$

$$u'/U_0 \ll 1 \tag{1.3}$$

where T_s, T_u and T_ε means time scale of duration of distortion, time scale of flow filed (which is time scale of non-linear interaction of the eddies), and viscous dissipation scale respectively. L_s and L are scale of flow field where distortion occurs and integral scale of turbulence respectively. U_0 and u' are representative mean velocity and rms value of turbulence respectively. The other notations' meanings are evident. The relationship $T_u \sim T_\varepsilon$ is inferred from the condition $Re_\lambda \gg 1$. In this case we can use well known Taylor's estimation $\varepsilon_T \sim u'^3/L$, then $T_\varepsilon \sim u'^2/\varepsilon_T \sim L/u' \sim T_u$ follows.

If conditions (1.1,2,3) are satisfied we can linearize Navier-Stokes equation[1-16)]. Frequently linearized perturbed vorticity equation is used, that is;

$$\frac{\partial \omega}{\partial t} + (\mathbf{U}\cdot\nabla)\omega = (\omega\cdot\nabla)\mathbf{U} \tag{1.4}$$

where instantaneous vorticity is decomposed as mean vorticity Ω and fluctuating vorticity ω. The idea of rapid distortion originated from Prandtl and theoretical treatment of the theory was due to Bachelor & Proudman[1-15)]. Much development of the rapid distortion theory was established by Hunt and also he applied this theory to the turbulence field around a bluff body[1-16)].

His main results shows that the streamwise turbulent velocity intensity changes as followings;

a) if $L/L_s \ll 1$, it increases as we approach the stagnation point,

b) if $L/L_s \gg 1$, it decreases as we approach the stagnation point and

c) if $L/L_s \sim O(1)$, when we are approaching the stagnation point, at first it increases and then decreases near the stagnation point.

Hunt explained these variation using the concept of blocking that is, turbulent large eddy can not maintain its free rotation if the distance between the eddy and the body surface becomes smaller than the eddy scale[1-16)]. Predictions of Hunt were confirmed by Bearman[1-35)] and Britter, Hunt & Mumford[1-36)]. Also related phenomena are examined by Gutmark, Wolfstein & Wygnanski[1-37)] using impinging jet, by Hunt, Rey & Arbey[1-38)] in case of stagnate region of a flat plate held perpendicular to the main flow in a wind tunnel. But no report treating three-dimensional case appeared without our's[1-19)] which will be discussed in detail in the next chapter.

Material diffusion field around two-dimensional bluff body has been examined theoretically by Burger[1-39)], Stumke[1-40)] and Hunt & Mulhearn[1-13)]. It is considered that Hunt & Mulhearn's analysis is most advanced but they still use following simplified assumptions,

$$u'/U_0 \ll 1 \tag{1.5}$$

$$(U_0/u'_0)^2 D/L_B U_0) \ll 1 \tag{1.6}$$

$$(L/u')/(L_B U_0) \ll 1 \tag{1.7}$$

where D is molecular difusion coefficient and L_B is the representative streamwise length of the body. Eq. (1.6) is required to neglect the molecular diffusion comparing turbulent diffusion and Eq. (1.7) means the presupposition of the rapid distortion theory. Main result of Hunt and Mulhearn can be stated as follows: provided that a line source or a point source is located on the stagnation streamline and far from the body, the decaying rate of mean concentration is relatively small than that of without the obstacle but near the obstacle the relationship is inverted that is the former decaying rate is larger than that of latter. In the case of point source this trend is more evident. Diffusion field around a circular cylinder has been studied by Puttock & Hunt[1-11], and by present authors[1-41]. Results obtained in these studies have confirmed well Hunt & Mulhearn's theoretical prediction[1-13]. Simplified considerations are given in Hunt's and also Hunt & Britter's papers[1-12),1-42], but until now no experiment has been done except our research[1-19].

1. 3 The construction of this study

In the experiment described in the next chapter, a sphere is placed in the decaying grid generated water turbulence and a point source axisymmetric plume of dye solution is diffusing along the stagnation line of the sphere. Mean velocity field, fluctuating velocity distribution are measured and mean rate of strain field is examined. Mean and fluctuating concentration fields are measured in detail and the effect of mean flow field distortion induced by the sphere on the concentration profile is discussed using the concentration equation. In chapter 3, concentration data are analyzed and the probability density function (hereafter referred as pdf) of concentration fluctuation is shown in front of and around the sphere. Also higher order statistics are discussed. Integral and dissipation scales of concentration are obtained and the relationship between them and the effect of distortion of the flow field is studied. Fractal property of the fluctuating concentration in a turbulent flow is the one of the recent topics in the field of diffusion study, in chapter 4 fractality of diffusing plume is clearly exhibited and the effect of flow distortion from the sphere on the fractal dimension is clarified.

References of chapter 1

1-1) Taylor, G.I., "Diffusion by continuous movements", *Proc. London Math. Soc.*, Ser.2, Vol.20 (1921), 196.

1-2) Moin, A.S. & Yaglom, A.M., *Statistical Fluid Mechanics, Volume 1,* MIT Press. (1971), 527.

1-3) Csanady, G.T., *Turbulent Diffusion in the Environment, Geophysics and Astrophysics Monographs, Vol.3,* D. Reidel Publishing Company (1973), 248.

1-4) Sakai, Y., "Experimental study on the diffusion by the light absorption method", *Ph.D. Dissertation* (1984), Nagoya University, Japan, (in Japanese).

1-5) Tsunoda, H., "Experimental study on the continuous point source plume in the shear flows", *Ph.D. Dissertation* (1988), Nagoya University, Japan, (in Japanese).

1-6) Liu, S., "Study in the turbulent diffusion field around the sphere", *Ph.D. Dissertation* (1992), Nagoya University, Japan, (in Japanese).

1-7) Hunt, J.C.R., Britter, R.E. & Puttock, J.S., "Mathematical models of dispersion of air pollution around buildings and hills", *Proc. IMA Symp. Math. Modelling Turbulent Diffusion Environ-*

ment, London Academic (1979), 145.

1-8) Snyder, W.H. & Hunt, J.C.R., "Turbulent diffusion from a point source in stratified and neutral flows around a three-dimensional hill - II. Laboratory measurements of surface concentrations. *Atmos. Environ.,* Vol.18, No.10 (1984), 1969.

1-9) Snyder, W.H., "Fluid modelling of pollutant transport and diffusion in stably stratified flows over complex terrain", *Annu. Rev. Fluid Mech.,* Vol.17 (1985), 239.

1-10) Cater, H.H. & Okubo, A., "A study of the physical process of movement and dispersion in Cape Kenndy Area", *Final Rep. U.S. At. Energy Comm. Contact No.AT(30-1)* (1965), 2973.

1-11) Puttock, J.S. & Hunt, J.C.R., "Turbulent diffusion from sources near obstacles with separated wakes - part I. An eddy diffusivity model", *Atmos. Environ.,* Vol.13, No.1 (1979), 1.

1-12) Hunt, J.C.R., "Turbulent diffusion from sources in complex flows", *Annu. Rev. Fluid Mech.,* Vol.17 (1985), 447.

1-13) Hunt, J.C.R. & Mulhearn, P.J., "Turbulent dispersion from sources near two-dimensional obstacles", *J. Fluid Mech.,* Vol.61, part 3 (1973), 245.

1-14) Hunt, J.C.R., Abell, C.J., Peterka, J.A. & Woo, H., "Kinematics studies of the flows around free or surface mounted obstacles, Applying topology to flow visualization", *J. Fluid Mech.,* Vol.86, part 1 (1978), 179.

1-15) Batchelor, G.K. & Proudman, I., "The effect of rapid distortion of a fluid in turbulent motion", *Quart, J. Mech. and Appl. Math.,* Vol.7, No.1 (1954), 83.

1-16) Hunt, J.C.R., "A theory of turbulent flow around two-dimensional bluff bodies", *J. Fluid Mech.,* Vol.61, part 4 (1973), 531.

1-17) Savill, A.M., "Recent developments in rapid-distortion theory", *Annu. Rev. Fluid Mech.,* Vol.19 (1989), 531.

1-18) Hunt, J.C.R. & Carruthers, D.J., "Rapid distortion theory and the 'problems' of turbulence", *J. Fluid Mech.,* Vol.212 (1990), 497.

1-19) Nakamura, I., Sakai, Y., Tsunoda, H. & Liu, S., "On the effect of the disturbance of a sphere on the point source diffusion process in grid-generated turbulence", *Proc. of 7th Symposium on Turbulent Shear Flows,* (1989), 14.5.1.

1-20) Liu, S., Tsunoda, H., Sakai, Y. & Nakamura, I., "Stochastic characteristics of a point-source plume diffusion field upstream of a sphere", *Trans. JSME,* Vol.57, No.541 (1991), 2976, (in Japanese).

1-21) Sakai, Y., Liu, S., Tsunoda, H. & Nakamura, I., "On the statistics of a point-source plume around a sphere", *Trans. JSME,* Vol.58, No.545 (1992), 51, (in Japanese).

1-22) Liu, S., Sakai, Y., Tsunoda, H. & Nakamura, I., "Multifractal feature of a diffusing plume and effect of distortion of flow due to a sphere on it", *Trans. JSME,* Vol.58, No.550 (1992), 1707, (in Japanese).

1-23) Nakamura, I., Sakai, Y., Tsunoda, H. & Liu, S., "Effect of flow distortion upon the diffusion process of a point source plume (characteristics of fluctuating velocity and concentration field) *Fluid and Heat Transfer Research,* Vol.25, No.2 (1990), 19, (in Japanese).

1-24) Hunt, J.C.R., Puttock, J.S. & Snyder, W.H., "Turbulent diffusion from a point source in stratified and neutral flows around a three-dimensional hill - Part I. Diffusion equation analysis", *Atmos. Environ.,* Vol.13 (1979), 1227.

1-25) Puttock, J.S., "Turbulent diffusion from sources near obstacles with separated wakes - Part II. Concentration measurements near a circular cylinder in uniform flow", *Atmos. Environ.,* Vol.13, No.1 (1979), 15.

1-26) Humphries, W. & Vincent, J.H., "An experimental investigation of the detection of airborne smoke in the wake bubble behind a disk", *J. Fluid Mech.,* Vol.73, part 3 (1976), 453.

1-27) Humphries, W. & Vincent, J.H., "Experiments to investigation of transport process in the near wakes of disks in turbulent air flow", *J. Fluid Mech.,* Vol.75, part 4 (1976), 737.

1-28) Ogawa, Y. & Oikawa, S., "A field investigation of the flow and diffusion around a model cube", *Atmos. Environ.,* Vol.16, No.2 (1982), 207.

1-29) Huber, A.H. & Snyder, W.H., "Wind tunnel investigation of the effects of a effluents from short adjacent stack", *Atmos. Environ.,* Vol.16, No.12 (1982), 2837.

1-30) Snyder, W.H. & Britter, R.E., "A wind tunnel study of flow and dispersion from upwind of three-dimensional hills", *Atmos. Environ.*, Vol.21, No.4 (1987), 735.
1-31) Prandtl, L., "Attaining a steady air stream in wind tunnels" *NACA Tech. Memo.*, No.726 (1933).
1-32) Taylor, G.I., "Turbulence in a contracting stream", *Zeit. f. Angew. Math. u. Mech.*, Vol.15 (1935), 91.
1-33) Townsend, A.A., "The uniform distortion of homogeneous turbulence", *Quart. J. Mech. and Applied Math.*, Vol.7, No.1 (1935), 104.
1-34) Tucker, H.I. & Reynolds, A.J., "The distortion of turbulence by irrotational plane strain", *J. Fluid Mech.*, Vol.32, part 4 (1968), 657.
1-35) Bearman, P.W., "Some measurements of the distortion of turbulence approaching a two-dimensional bluff body", *J. Fluid Mech.*, Vol.53, part 3 (1972), 451.
1-36) Britter, R.E., Hunt, J.C.R. & Mumford, J.C., "The distortion of turbulence by a circular cylinder", *J. Fluid Mech.*, Vol.92, part 2 (1979), 269.
1-37) Gutmark, E., Wolfshtein, M. & Wygnanski, I., "The plane turbulent impinging Jet", *J. Fluid Mech.*, Vol.88, part 4 (1978), 737.
1-38) Huot, J.P., Rey, C. & Arbey, H., "Distortion of turbulence approaching a plate held normal to the flow", *Phys. Fluids*, Vol.27, No.3 (1984), 541.
1-39) Burger, W., "Ein Verfahren zur Berucksitchtingung des Einflusses von Gebauden auf die Schadgasusbreitung in der Atmosphere", *Staub*, Vol.24 (1964), 223.
1-40) Stumke, H. "Inclusion of simplified types of terrain in calculation of turbulence diffusion of gas from chimneys", *Staub*, Vol.24 (1964), 175.
1-41) Tsunoda, H., Sakai, Y., Nakamura, I. & Liu, S., "The effect of a circular cylinder on the diffusion of matter by a plume", *J. Fluid Mech.*, Vol.246 (1993), 419.

2. Effects of Distortion of Mean Flow due to a Sphere on Turbulence and Concentration Field

2. 1 Introduction

In recent years, studies on the changing process of turbulence caused by the distortion of the mean velocity field have been steadily increasing[2-1)~2-8)]. The strong diffusivity of turbulence, which gives rise to rapid mixing of matter, is one of the most important features of all turbulent flows, and so it is expected that the distortion of the flow must certainly have direct influences on the diffusion process of matter[2-9)]. In reference to the flow field around obstacles, Britter et al.[2-10)] and Bearman[2-11)] have obtained the turbulence statistics around a circular cylinder and a two-dimensional flat plate, respectively. Many investigations have been conducted on the diffusion process of matter for cases of cylinders[2-4)~2-7),2-12),2-13)], ridges[2-14)], disks[2-15),2-16)], buildings[2-17),2-18)], hills[2-19)~2-21)], and such (see chapter 1). However, the effect of turbulence distortion by the mean flow upstream of these obstacles has hardly been investigated. Also, to our knowledge, there are still very few studies on the concentration fluctuation field around obstacles except two dimensional limited case[2-4)~2-8)]. Various theoretical analyses[2-1),2-9),2-20)~2-23)] on two-dimensional obstacle problems have been presented, but comparison with the experimental results has been insufficient. Theoretical studies on three-dimensional body problems have also displayed little progress to date. In this research, as a first step to further research on three-dimensional problems, detailed experimental investigations have been carried out in the fields of velocity and concentration around the sphere. Special attention has been given to the varying process of streamwise turbulence and the concentration fluctuation intensities along the upstream stagnation streamline. The respective budget equations have been used to explain these curves.

Nomenclature of chapter 2

x, y, z	:	main streamwise, horizontal and vertical coordinates (see Fig. 2.1)
r, θ	:	radial coordinate and zenithal angle (see also Fig. 2.1)
U, W	:	x, z components of the mean velocity vector
U_0	:	mean velocity of the main stream
u'	:	main streamwise velocity fluctuation rms value
Γ, γ'	:	mean concentration and concentration fluctuation rms value
Γ_j	:	initial concentration at the nozzle exit
d, a	:	diameter and radius of the sphere
subscript		
c	:	value on the plume axis

2. 2 *Experimental instruments and coordinate systems*

Figure 2.1 shows the experimental arrangement and the coordinate systems used. For experimental instruments, a water channel with a 250 mm × 250 mm cross-section and a 1920 mm length was employed. At the entrance to the channel, a biplanar square grid with a mesh size of 10 mm and a bar diameter of 2 mm were installed so that roughly isotropic turbulence was generated downstream of the grid plane. Diffusion material (a water solution of direct dye, Lionol blue (C.I. Direct Blue 86, C.I.74180)) was released from a nozzle 2 mm in diameter, which had been soldered to a pipe that itself provided one of the vertical bars. The release velocity was adjusted to 1.7 times the mean velocity of the main stream to compensate the flow for the defect of the mean velocity caused by the wake of the nozzle body. The maximum initial concentration of this dye solution was adjusted to $\Gamma_j = 1.0$ g/l in the present experiments, so that the maximum density of diffusing material is about 1.001 g/cm^3. Consequently, the difference between diffusing material and surrounding pure water is very small and its effect on the concentration field is almost negligible.

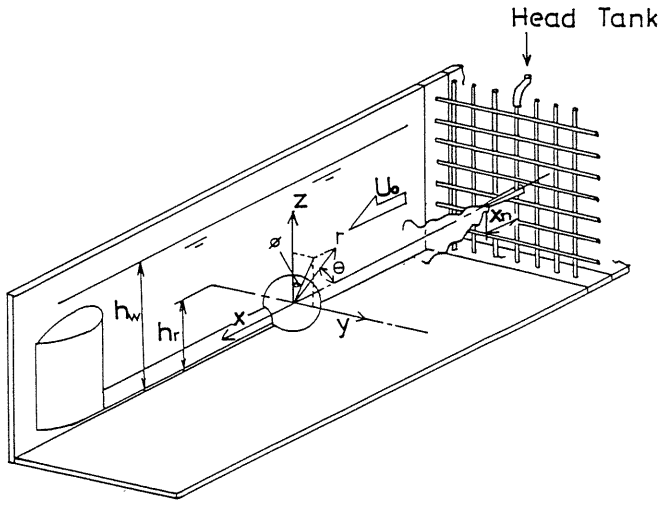

Fig. 2.1 Experimental arrangement and coordinates.

As shown in Fig. 2.1, a sphere with a diameter of 60 mm was supported by a brass rod 14 mm in diameter and 221 mm in length, which had been fixed to the stay in the cross-section of the main streamlines. This sphere is movable in y and z directions, so it is easy to adjust the cross-sectional position of the sphere to ensure that its center is located on the axis of the plume. The location of the sphere downstream of the grid plane was 600 mm. Axisymmetries of the velocity field and the concentration field were ascertained by a preparatory test in the cross-section 4 mm upstream of the stagnation point of the sphere. The Reynolds number Re_d, which is defined by $Re_d = U_0 d/\nu$, was about 5960; calculated from the main stream velocity $U_0 = 12.9$ cm/s, the diameter of the sphere $d = 60$ mm and the kinematic viscosity ν of water at 10°C, which is 1.307×10^{-6} m^2/s. Furthermore, to maintain the steadiness of the mean velocity field, the depth of the water was kept at 160 mm.

Another important parameter which gives much influence to the fine scale structure of concentration field is the molecular diffusivity of dye D. Although the precise value of molecular diffusivity is unfortunately unknown, here the molecular Schmidt number $S_c = \nu/D$ is supposed to be about 3.8×10^3[2-7].

For the mean velocity measurements, we used a Laser Doppler velocimeter[2-24] (KANOMAX, Model 27-0900 series) equipped with a frequency shifter (KANOMAX, Model 27-0980), and for the turbulence intensity a normal "I"-shaped hot-film probe was chosen (TSI, Model 1210-60W; sensor element diameter, 152 μm). To measure the mean concentration and the concentration fluctuation we adopted an optical fiber probe[2-25], by means of which the concentration levels can be determined from the Lambert-Beer's law. A brief sketch of the sensor of the optical fiber probe is given in Fig. 2.2. Laser beam produced by a semiconductor laser diode, passing through the optical fiber of ϕ0.1 mm is reflected at the tip of the probe by the chromium-coating, and is then led to the sensing part, where the light is absorbed by the diffusing material. The light power spectrum of semiconductor laser has a peak value at a wavelength of 670 nm, where the diffusing material, the Lionol blue dye solution is found to have its best absorbability. The output laser light, carrying information about the concentration field, is guided to a photo-diode, by which the light signals are converted into electric ones. The sampling volume of the probe is estimated at 2.4×10^{-6} cm^3, and the spacing between two fibers at the tip of the probe is about 0.3 mm. Because the Kolmogorov scale is 1 mm or so (see section 4.2 in chapter 4), this probe is expected to be sufficiently resolutive to investigate the fine structure of the diffusion field around the Kolmogorov scale.

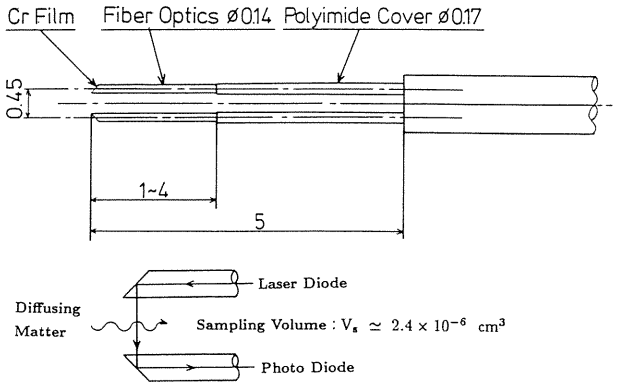

Fig. 2.2 Schematic sketch of the light probe for concentration measurement.

Several important parameters[2-1),2-22),2-23)] of the velocity field and the concentration field in the absence of the sphere were measured at the sphere position with the following results: $u'/U_0 = 1.4\%$, $L/d = 0.19$, $b_\Gamma/d = 0.16$, where L represents the longitudinal integral length scale which was obtained by means of the auto-correlation analysis of the turbulent velocity, and b_Γ is the half width across the plume. In this experiment, measurements were made only when these parameters were constant.

Fig. 2.3 shows the photograph for the plume passing by the sphere. It can be supposed that the diffusing plume is markedly distortion near the stagnation point.

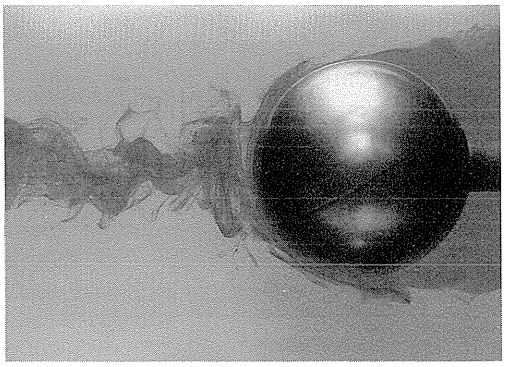

Fig. 2.3 Photograph for the plume passing by a sphere. Note that the stretching and folding of the diffising material in front of a sphere.

2. 3 Experimental results and discussions

2. 3. 1 Mean velocity field

For the mean velocity field, detailed measurements of U and W were conducted at various zenithal angles as shown in Figs. 2.4(a) and (b). The solid line in the figure indicate the mean velocity profiles of the potential flow around the sphere. From these figures, it is found that the profiles of both U and W are in good agreement with those of the potential flow in the range $\theta < 67.5°$[2-9)]. This may be cecause the boundary layer developing on the wall of the sphere is laminar and the measurement of velocity was made outside of the boundary layer (the thickness of the boundary layer is estimated to be less than 1 mm). As θ increases, especially in the region affected by the flow separation (which is likely to take place at about $\theta = 90°$), the velocity profiles near the surface begin to deviate from those of the potential flow.

The mean flow streamlines obtained by means of interpolation to experimental data are shown in Fig. 2.5. For clarity, the broken-line square window in the figure has been enlarged and shown at the upper left. Here, Ψ denotes the Stokes' stream function which is defined by

$$\Psi = \int_a^r r' U_\theta \sin\theta dr' \tag{2.1}$$

where U_θ is the tangential component of the mean velocity. Arrows in the figure represent

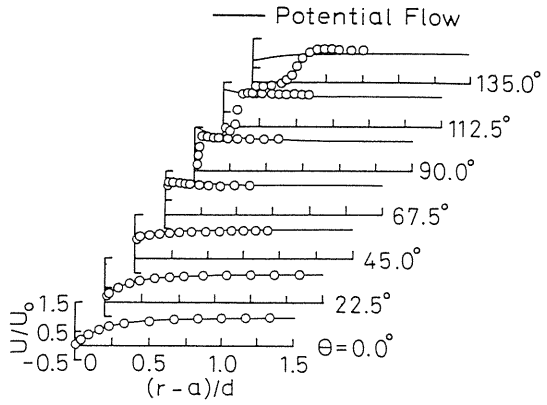

Fig. 2.4(a) Radial distributions of the horizontal mean velocity component U at each θ.

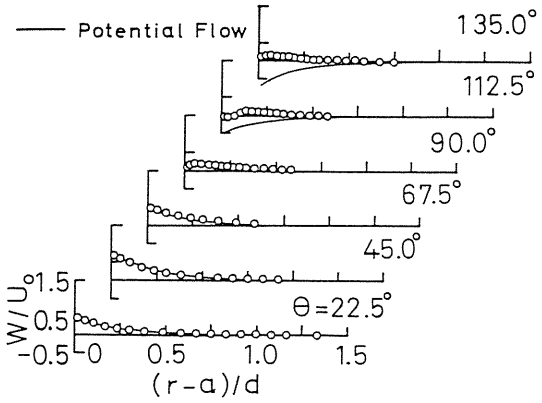

Fig. 2.4(b) Radial distributions of the vertial mean velocity component W at each θ.

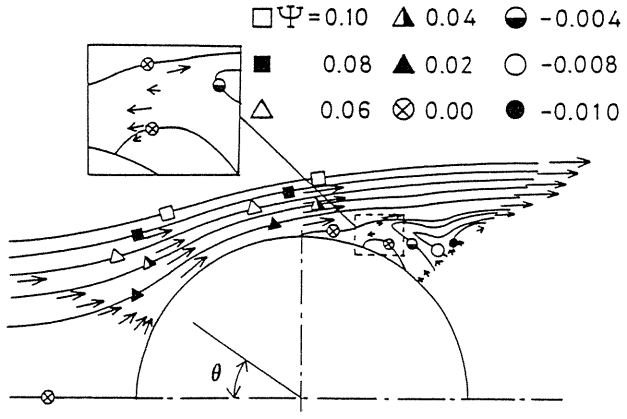

Fig. 2.5 The streamlines of the mean flow.

the mean velocity vectors. The mean flow separation is found to occur near the top of the sphere ($\theta = 90°$), and there is a kind of separation bubble-like structure on the surface inside the separated flow region[2-26].

From the data of the velocity field, the deformation tensor of the flow could be calculated, which is defined by

$$S = \begin{bmatrix} 2\frac{\partial U}{\partial x} & \frac{\partial U}{\partial y} + \frac{\partial V}{\partial x} & \frac{\partial U}{\partial z} + \frac{\partial W}{\partial x} \\ \frac{\partial V}{\partial x} + \frac{\partial U}{\partial y} & 2\frac{\partial V}{\partial y} & \frac{\partial V}{\partial z} + \frac{\partial W}{\partial y} \\ \frac{\partial W}{\partial x} + \frac{\partial V}{\partial z} & \frac{\partial W}{\partial y} + \frac{\partial V}{\partial z} & 2\frac{\partial W}{\partial z} \end{bmatrix} \tag{2.2}$$

The orientation and the magnitudes of the three principal components of the normalized deformation tensor are shown in Fig. 2.6(a), where we express their magnitudes by the lengths of the arrows, and their directions by the orientations of the arrows in the figure, except for the components normal to the paper, i.e., the y components whose magnitudes are denoted by the radii of the broken circles. The relationship between the length of the arrow and the magnitude of the principal component could be determined from the reference arrow shown in the upper left of Fig. 2.6(a), which denotes a magnitude of 10. From Fig. 2.6(a), it is found that for $\theta < 90°$ the flow is suppressed radially, and stretched both zenithally and azimuthally. It is also obvious that the normal distortion rates of suppression of the flow near the stagnation point are on the order of 10; hence, the plume passing by the sphere may be markedly distorted. The support for this speculation is also given in Fig. 2.3.

Figure 2.6(b) gives the same diagram for the potential flow field around the sphere as one for the measured flow field (shown Fig. 2.6(a)). It is found that as long as θ is smaller than 60 degree, the directions of the principal axes and the magnitudes of the principal components of the deformation tensors are almost the same as those of the potential flow except very close to the surface of the sphere.

Here in order to understand more specifically how strongly the flow is distorted near the sphere, we investigated the distribution of the magnitudes of the tree principal components of the normalized deformation tensor along the stagnation streamline. The results are shown in Fig. 2.7, where it is noted that because the flow is axisymmetric in this case, the y, z components could be considered as the same one and this figure has been drawn from the mean velocity data. It is clear in Fig. 2.7 that the distortion rate is rapidly increasing as the sphere is approached, and that it is reasonable to infer that the diffusion field should receive appreciable effect of the flow distortion close to the sphere.

2. 3. 2 Fluctuation velocity field

Figures 2.8 (a) and (b) show the distributions of the velocity rms value along the stagnation streamline and along the circumference of a circle of $r/d = 0.53$, respectively. Since the relative intensity of turbulence is quite small (less than 2.5%), we can refer to these results as the distribution of turbulence rms value in the local tangential direction of the mean streamline. In Fig. 2.8 (a), the data were normalized by the far upstream rms value u'_{xo} at $(x + a)/d = -2.0$ where the disturbance by the sphere is negligible. And further the results in the absence of the sphere[2-27] are also plotted for comparison. It is clear from Fig. 2.8 (a) that

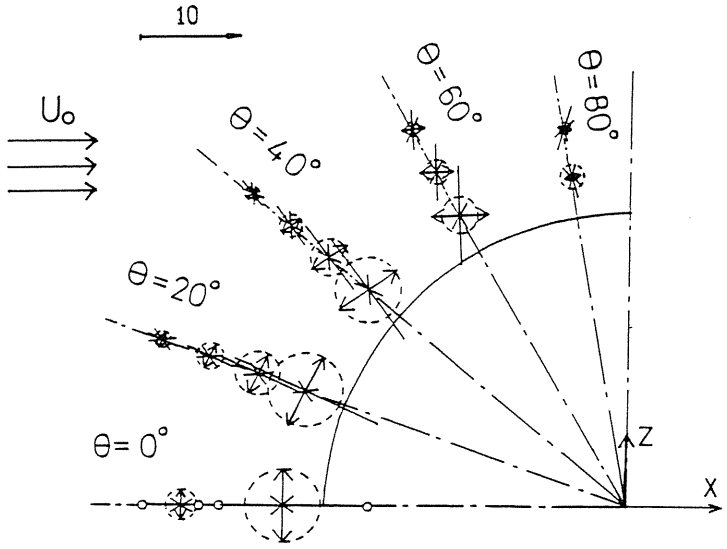

(a)

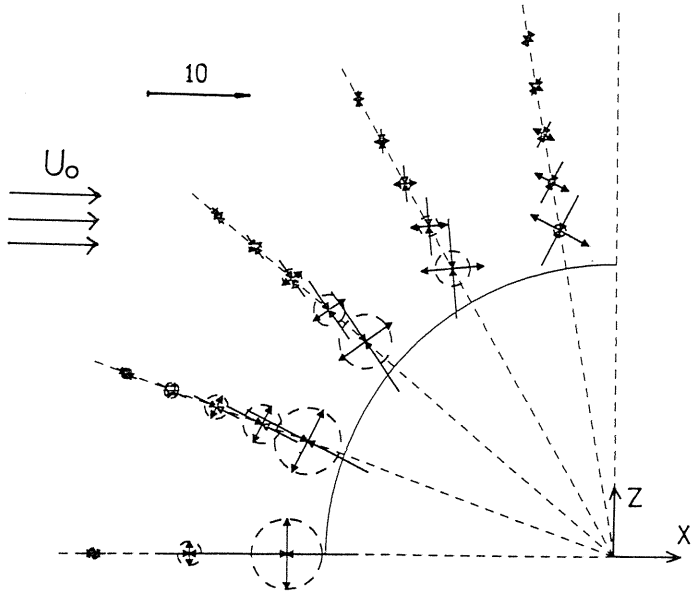

(b)

Fig. 2.6 Distribution of the normalized deformation tensor around the sphere.
(a): in case of the measured mean velocity field.
(b): in case of the potential flow field.

as the sphere is approached, u' begins first to increase at about $(x+a)/d=-0.5$ as comparison with the case without the sphere and then decays again close to the surface by the blocking effect[2-1]. These phenomena can be qualitatively explained by means of the turbulence energy equation as follows.

The energy balance equation for the longitudinal turbulence on the stagnation line in cylindrical coordinate is

$$U_x\frac{\partial\left(\overline{u_x^2}/2\right)}{\partial x}=-\overline{u_x^2}\frac{\partial U_x}{\partial x}-\left[\overline{u_x^2\frac{\partial u_x}{\partial x}}+\overline{\frac{u_\phi u_x}{\sigma}\frac{\partial u_x}{\partial x}}+\overline{u_\sigma u_x\frac{\partial u_x}{\partial x}}\right]$$
$$+\left[\overline{\frac{1}{\rho}p\frac{\partial u_x}{\partial u_x}}-\frac{1}{\rho}\frac{\partial(\overline{pu_x})}{\partial x}\right]$$
$$+\nu\left[\frac{\partial^2}{\partial x^2}\left(\frac{1}{2}\overline{u_x^2}\right)+\frac{\partial^2}{\partial\sigma^2}\left(\frac{1}{2}\overline{u_x^2}\right)\right]$$
$$-\nu\left[\overline{\left(\frac{\partial u_x}{\partial x}\right)^2}+\overline{\left(\frac{\partial u_x}{\partial\sigma}\right)^2}+\frac{1}{\sigma^2}\overline{\left(\frac{\partial u_x}{\partial\phi}\right)^2}\right] \tag{2.3}$$

where we use the coordinate system (σ, ϕ, x) for convenience instead of a usual cylindrical coordinate system (r, θ, z) and denote the radial and angular coordinate in the y-z plane by σ and ϕ, respectively. The mean and fluctuating velocity components in (σ, ϕ, x) direction are defined as (U_σ, U_ϕ, U_x) and (u_σ, u_ϕ, u_x), respectively. Furthermore, the stationary and axisymmetry of the mean flow are assumed in Eq. (2.3). In the right hand side of this equation, the first term states the production of the streamwise turbulence energy, the second and forth term are the turbulent and viscous diffusion term respectively, and the fifth term expresses the viscous dissipation. In the third term on the right-hand side of Eq. (2.3), $\overline{p(\partial u_x/\partial x)}/\rho$ plays a role which returns an anisotropic turbulence to an isotropic one through the interaction of the pressure and the velocity fluctuations, and $(-\partial\overline{pu_x}/\partial x)/\rho$ expresses the transport of turbulence energy by the pressure fluctuation. The production term has a positive contribution because of $\partial U_x/\partial x<0$ on the stagnation line, and it is clear that the dissipation term is always negative. On the other hand, the signs of two transport terms through the velocity fluctuation and the viscous stress are considered to change locally. The effect of the pressure-velocity cross correlation term $(-\partial\overline{pu_x}/\partial x)/\rho$ may be neglected in the far upstream region where the distance from the sphere surface is greater than the integral scale of turbulence L, but within that distance it probably has a negative contribution due to the blocking effect[2-1] of the surface so that the streamwise turbulence will decay.

Now, we consider qualitatively the change of u'_x on the stagnation streamline in Fig. 2.8 (a), by dividing it into three regions on the basis of Eq. (2.3). In the first region $((x+a)/d<-0.5)$ far upstream from the sphere, the viscous dissipation is considered to cause mainly a decrease in the longitudinal turbulence component because the turbulence field in upstream flow is approximately isotropic and the turbulence production is zero here. In the next region $(-0.5<(x+a)/d<-0.2)$ where the distance from the sphere is relatively small but still larger than the scale of turbulence L, the energy of the mean flow is transferred to the

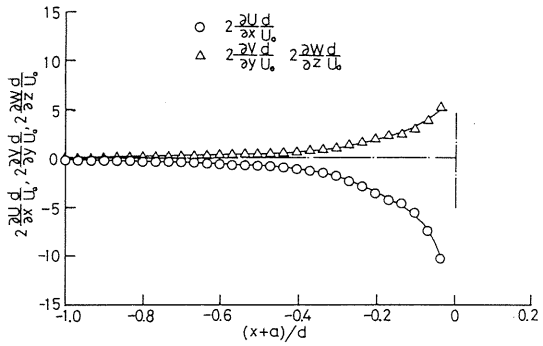

Fig. 2.7 The principle components of the normalized deformation tensor on the stagnation streamline.

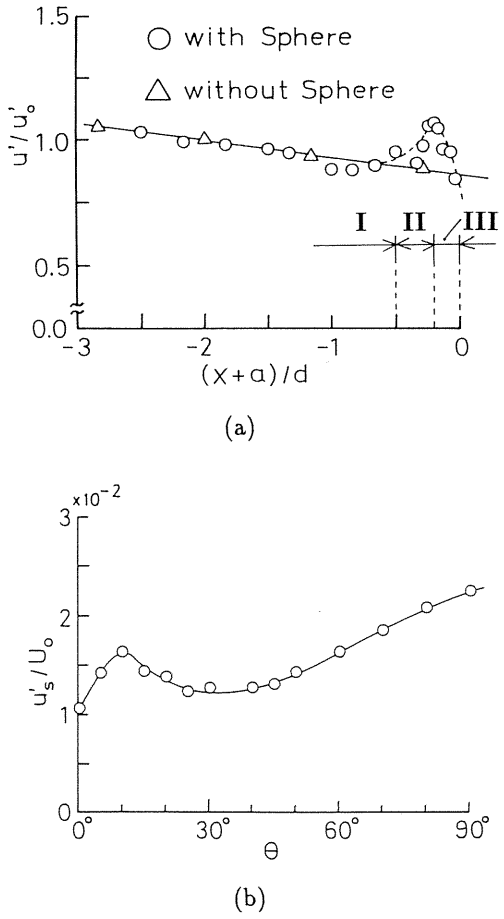

Fig. 2.8 The distribution of the streamwise velocity fluctuation rms value.
(a): on the stagnation line.
(b): along the circumference of a circle of $r/d = 0.53$.

turbulence through the vorticity distortion by the mean motion, and thus it is expected the downstrem variation of u'_x will turn into an amplification. Finally, within the distance smaller than L ($-0.2 < (x+a)/d < 0$), the blocking effect of the body surface surpasses the vorticity distortion effect so that u'_x decreases again as the sphere is approached.

Now we turn our attention to the circumferential distribution of the turbulence rms value shown in Fig. 2.8(b). In the figure, the abscissa is the zenithal angle from the stagnation point (see Fig. 2.1), and u'_s of the ordinate denotes the rms value of velocity component in the mean stream direction. From the figure, we can clearly find the maximum value of u'_s around $\theta = 10°$.

2. 3. 3 *Mean concentration field*

Figure 2.9 shows the profiles of the mean concentration along y axis in the given 5 cross-sections, where the abscissa and ordinate are non-dimensionalized by the half-width of the mean concentration profile b_Γ and the mean concentration on the centerline of the plume Γ_c, respectively. And the solid line in the figure expressed the Gaussian distribution. It is found that at the region of $-0.69 \leq x/d \leq -0.51$, the profile becomes to get out of the self-similar shape in the downstream direction. Although not presented here, we also investigates the variation of profile of the mean concentration along z axis, and found that its variatio shows the same tendency as one given in Fig. 2.9.

In Fig. 2.10, the mean concentration distribution along the stagnation streamline of the flow has been given, accompanied by the one in the absence of the sphere[2-27]. Comparison

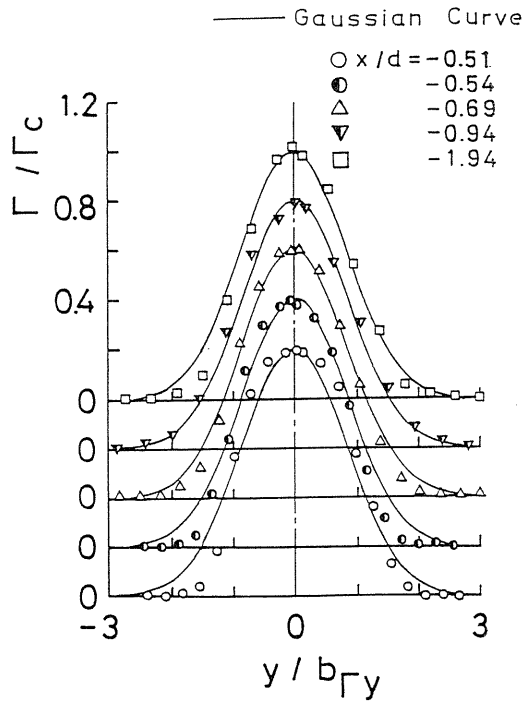

Fig. 2.9 The cross-sectional profiles of the mean concentration upwind of the sphere.

lets us conclude that there is no perceptible difference between them over the major part of the x range measured. However, in the vicinity of the stagnation point, there is a slight rising of the mean concentration magnitude in the case of a sphere being put in the flow against the plume. We suppose that this phenomenon may be associated with the intermittency of the concentration signals, but in the present paper no satisfactory explanation could be given even when the gradient diffusion model has been introduced to the turbulent diffusion terms.

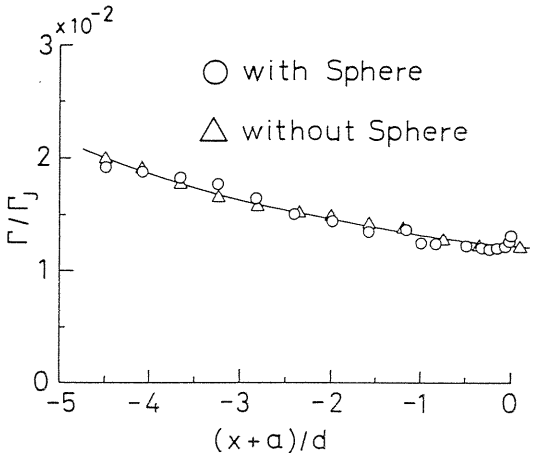

Fig. 2.10 The downstream variation of the mean concentration on the stagnation line.

Figure 2.11 gives us the radial profiles of the mean concentration at various zenithal angles. The mean concentration magnitudes near the sphere surface can be found to become greater than those far away from the surface as θ increases. In the meantime, the plume becomes narrower and narrower as a result of the streamwise stretching of the flow. When θ is greater than 90 degrees, the radial position of the maximum mean concentration moves outwards away from the sphere surface because of the flow separation, whereas the near surface profiles still has such a flat shape that one can say that the uniformalization of the concentration field by the molecular diffusion has already fairly progressed near the surface. Using the data on the mean concentration field, we have obtained the contour lines of the mean concentration field which have been shown in Fig. 2.12. It is shown that near the stagnation point, the contour lines are approximately parallel to x axis. However, the most interesting finding from Fig. 2.12 is that in the separated flow area, some maximum magnitude domains exist. The cause of these domains remains unclear at present, but if we make a comparison of these contours with the mean streamlines, it is reasonable to postulate that these domains have close relations with the vortex-like structures in the mean streamlines.

2. 3. 4 Fluctuation concentration field

Figure 2.13 shows the variation of the concentration fluctuation rms value along the stagnation streamline. Where γ'_0 is the value at $(x + a)/d = -2.0$. The conclusion we can draw from this figure is that in the vicinity of the stagnation point, the concentration fluctuation

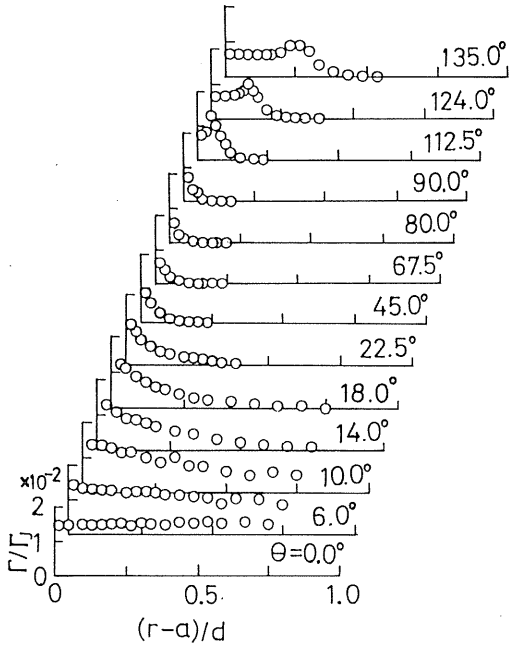

Fig. 2.11 The radial profiles of the mean concentration at various zenithal angles.

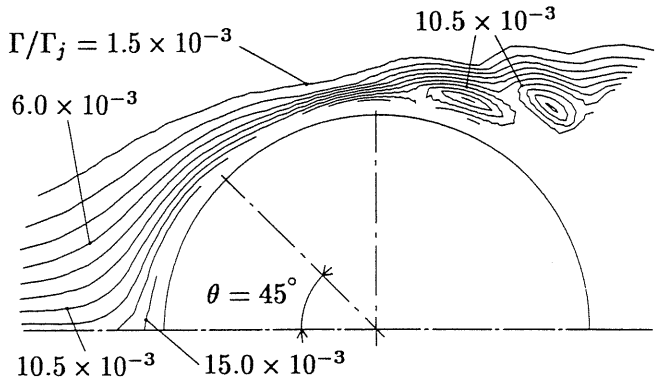

Fig. 2.12 The contour lines of the mean concentration field.

rms value decreases rapidly as the sphere surface is approached. To find an explanation for this phenomenon, we shall examine the balance equation of $\overline{\gamma^2}$ in the following discussion.

Eq. (2.4) gives the balance equation of $\overline{\gamma^2}$ on the stagnation line,

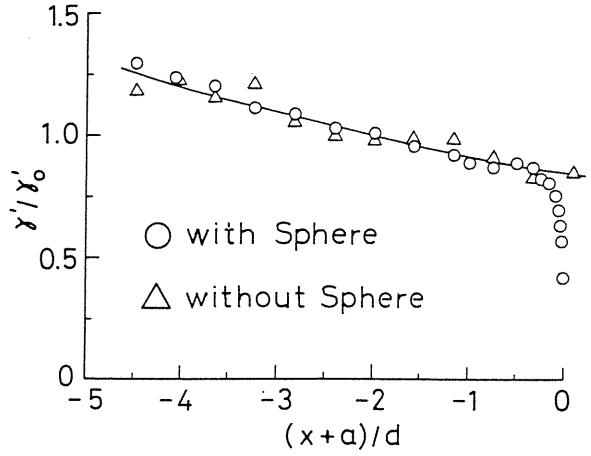

Fig. 2.13 The variation of the concentration fluctuation rms value on the stagnation streamline.

$$U_x \frac{\partial \overline{\gamma^2}}{\partial x} = -\left[\overline{u_x \frac{\partial \gamma^2}{\partial x}} + \overline{u_\sigma \frac{\partial \gamma^2}{\partial \sigma}} + \overline{\frac{u_\phi}{\sigma} \frac{\partial \gamma^2}{\partial \phi}} \right]$$
$$- 2D_m \left[\overline{\left(\frac{\partial \gamma}{\partial x}\right)} + \overline{\left(\frac{\partial \gamma}{\partial \sigma}\right)} + \overline{\left(\frac{1}{\sigma^2} \frac{\partial \gamma}{\partial \phi}\right)} \right] \tag{2.4}$$

where the term on the left-hand side of the equation is the convection term, while the first term on the right-hand side denotes the turbulent diffusion, and the second the dissipation of $\overline{\gamma^2}$. Because the gradient of the mean concentration along x axis is small, the production term $-2\overline{u_x\gamma}(\partial\Gamma/\partial x)$ has been removed from the equation. It is reasonable that we neglect the molecular diffusion too.

Among the causes of the rapid attenuation of γ' near the stagnation point, there are three important factors: the rapid decrease of the x-wise mean flow velocity (effect of convection), the distortion of the flow and the blockage effect[2-1)] produced by the sphere surface, which are supposed to accelerate the molecular diffusion (effect of dissipation), and the transportation of the concentration fluctuation intensity by the turbulent velocity (effect of turbulent diffusion). However, it must be pointed out that the above three factors should be acting upon $\overline{\gamma^2}$ as a whole instead of individually.

Figure 2.14 shows the profiles of the concentration fluctuation rms values along y axis in the given 5 cross-sections. We can find that when x/d is greater than -0.69, the profiles possess double peaks which are likely to be closely associated with the rapid attenuation of γ' in the vicinity of the stagnation point shown in Fig. 2.13. One more finding of interest from Fig. 2.14 is that the position at which the double peak type of profiles comes into being, that is $x/d \sim -0.69$ ($(x+a)/d \sim 0.2$), shows a surprising agreement with the one at which the velocity fluctuation u' starts its attenuation again after it passes the peak magnitude.

The radial profiles of the concentration fluctuation rms values at the given angles have

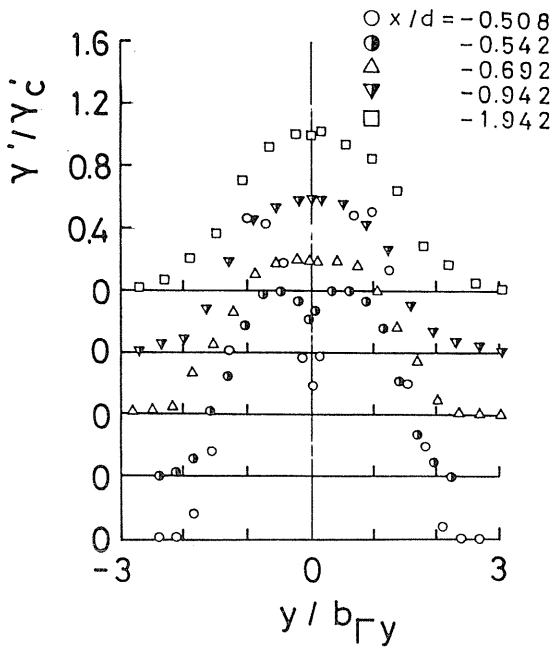

Fig. 2.14 The cross-sectional profiles of the concentration fluctuation rms value upwind of the sphere.

been shown in Fig. 2.15. When θ is smaller than 18 degrees, attenuation of the concentration fluctuation occurs near the surface of the sphere, but when θ is greater than 22.5 degrees, this kind of attenuation vanishes completely. It is also found that, at the positions of θ greater than 112.5 degrees, the radial position of the maximum magnitude moves away from the sphere surface, though it still coincides with the position where the radial mean concentration gradient attains its peak value. This phenomenon can be attributed to the result of the flow separation.

By interpolating the experimental data, we can draw the contour lines of the concentration fluctuation field, which have been given in Fig. 2.16. Just as in the mean concentration field, similar maximum magnitude domains clearly exist in the concentration fluctuation field as well.

2. 4 Conclusions

(1) When the relative rate of the turbulence to the mean velocity is small enough as in the present research, the profiles of the mean velocity will show nearly the same shape as in the potential flow if θ is small enough that the separation effect remains negligible.

(2) The distribution of x components of the velocity fluctuation on the stagnation line possesses a unique shape, for as the stagnation point is approached, the magnitude of u' increases more than in the absence of the sphere around $(x + a)/d = -0.5$; then, after it has passed its peak value, it steeply decays again near the stagnation point. On the other hand, in the circumferential distribution of rms value of turbulence velocity component in the mean stream direction at $r/d = 0.5$, there exists the maximum value around $\theta = 10°$

(3) The mean concentration distribution on the stagnation line has no remarkable difference

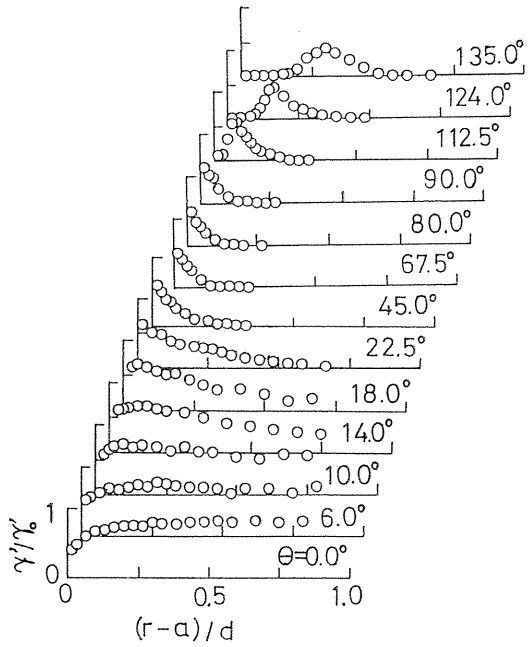

Fig. 2.15 The radial profiles of the concentration fluctuation rms value at various zenithal angles.

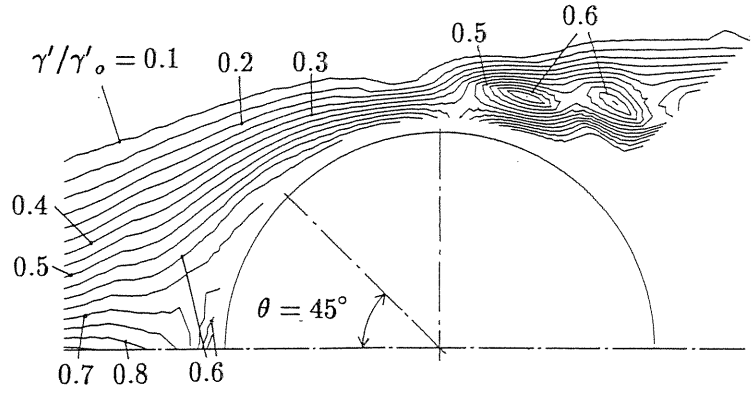

Fig. 2.16 The contour lines of the fluctuating concentration field.

from the one in the absence of the sphere except in the vicinity of the stagnation point. The concentration fluctuation distribution has a rapid attenuation near the stagnation point, and as a result, the cross profiles of γ' posses double peaks.

(4) In the separated flow region, there are some maximum magnitude domains both in the mean concentration field and in the concentration fluctuation field.

References of chapter 2

2-1) Hunt, J.C.R., "A theory of turbulent flow around two-dimensional bluff bodies", *J. Fluid Mech.,* Vol.61, part 4 (1973), 625.

2-2) Savill, A.M., "Recent developments in rapid-distortion theory", *Ann. Rev. Fluid Mech.,* Vol.19 (1989), 531.

2-3) Hunt, J.C.R. & Carruthers, D.J., "Rapid distortion theory and the 'problems' of Turbulence", *J. Fluid Mech.,* Vol.212 (1990), 497.

2-4) Nakamura, I., Sakai, Y., Tsunoda, H. & Arao, T., "The disturbance effect of a circular cylinder on the diffusion of matter by a plume from a point source in grid-generated turbulence (1st report, Characteristics of velocity and mean concentration field)", *Trans. JSME,* Vol.53, No.487 (1987), 765, (in Japanese).

2-5) Nakamura, I., Sakai, Y., Tsunoda, H. & Arao, T., "The disturbance effect of a circular cylinder on the diffusion of matter by a plume from a point source in grid-generated turbulence (2nd report, Characteristics of the fluctuating concentration field)", *Trans. JSME,* Vol.53, No.487 (1987), 774, (in Japanese).

2-6) Tsunoda, H., Sakai, Y., & Nakamura, I., "The disturbance effect of a circular cylinder on the diffusion of matter by a plume from a point source in grid-generated turbulence (3rd report, Characteristics of the conditional statistics)", *Trans. JSME,* Vol.54, No.503 (1988), 1581, (in Japanese).

2-7) Tsunoda, H., Sakai, Y., Nakamura, I. & Liu, S., "The effect of a circular cylinder on the diffusion of matter by a plume", *J. Fluid Mech.,* Vol.246 (1993), 419.

2-8) Huot, J.P., Rey, C. & Arbey, H., "Distortion of turbulence approaching a plate held normal to the flow", *Phys. Fluids,* Vol.27, No.3 (1984), 541.

2-9) Hunt, J.C.R. & Mulhearn, P.J., "Turbulent dispersion from sources near two-dimensional obstacles". *J.Fluid Mech.,* Vol.61, part 3 (1973), 245.

2-10) Britter, R.E., Hunt, J.C.R. & Mumford, J.C., "The distortion of turbulence by a circular cylinder". *J. Fluid Mech.,* Vol.92, part 2 (1979), 269.

2-11) Bearman, P.W., "Some measurements of the distortion of turbulence approaching a two-dimensional body", *J. Fluid Mech.,* Vol.53, part 3 (1972), 451.

2-12) Puttock, J.S. & Hunt, J.C.R., "Turbulent diffusion from sources near obstacles with separated wakes - part I. An eddy diffusivity model," *Atmos. Environ.,* Vol.13, No.1 (1979), 1.

2-13) Puttock, J.S., "Turbulent diffusion from sources near obstacles with separated wakes - part II. Concentration measurements near a circular cylinder in uniform flow", *Atmos. Environ.,* Vol.13, No.1 (1979), 15.

2-14) Arya, S.P.S., Shipman, M.S. & Courney, L.Y., "An experimental investigation of flow and diffusion in the disturbed boundary layer over a ridge -- II. Diffusion from a continuous point source", *Atmos. Environ.,* Vol.15, No.7 (1981), 1185.

2-15) Humphries, W. & Vincent, J.H. "An experimental investigation of the detention of airborne smoke in the wake bubble behind a disk", *J. Fluid Mech.,* Vol.73, part 3 (1976), 453.

2-16) Humphries, W. & Vincent, J.H., "Experiments to investigate transport processes in the near wakes of disks in turbulent air flow", *J. Fluid Mech.,* Vol.75, part 4 (1976), 737.

2-17) Ogawa, Y. & Oikawa, S., "A field investigation of the flow and diffusion around a model cube", *Atmos. Environ.,* Vol.16, No.2 (1982), 207.

2-18) Snyder, W.H. & Lawson, R.E., "Determination of a Necessary Height for a Stack close to a Building - A wind tunnel study", *Atmos. Environ.,* Vol.10, No.9 (1976), 683.

2-19) Castro, I.P & Snyder, W.H., "A wind tunnel study of dispersion from sources downstream of three-dimensional hills", *Atmos. Environ.,* Vol.16, No.8 (1982), 1869.

2-20) Snyder, W.H. & Britter, R.E., "A wind tunnel study of the flow structure and dispersion from sources upwind of three-dimensional hills", *Atmos. Environ.,* Vol.21, No.4 (1987), 735.

2-21) Snyder, W.H. & Hunt, J.C.R., "Turbulent diffusion from a point source in stratified and neutral flows around a three-dimensional hill - II. Laboratory measurements of surface concentrations",

Atmos. Environ., Vol.18, No.1 (1979), 1969.
2-22) Hunt, J.C.R., Puttock, J.S. & Snyder, W.H., "Turbulent diffusion in neutral flows around a three-dimensional hill - part I. Diffusion equation analysis", *Atmos. Environ.*, Vol.13 (1979), 1227.
2-23) Hunt, J.C.R., "Turbulent diffusion from sources in complex flows", *Ann. Rev. Fluid Mech.*, Vol.17 (1985), 447.
2-24) Durst, F., Melling, A. & Whitelaw, J.H., *Principles and Practice of Laser-Doppler Anemometry*, Academic Press (1976).
2-25) Nakamura, I., Miyata, M. & Sakai, Y., "On a method of the concentration measurement by use of light absorption law", *Bull. JSME*, Vol.26, No.218 (1983), 1357.
2-26) Dallman, U. & Schulte-Werning, B., "Topological changes of axisymmetric and non-axisymmetric vortex flows", *Proc. of the IUTAM Symposium at Cambridge University* (1989), 372.

3. Distortion Effects of Flow due to a Sphere on the Structure of Axisymmetric Diffusion Plume

3. 1 Introduction

In this chapter, reported are mainly results on the characteristics of conventional and conditional pdf, the concentration detecting frequency and the auto-correlation function of the concentration fluctuation signal.

Here we notice that there is almost no report on the conditional statistics of the concentration field in particular around the three dimensional body, although we can find some references with regard to a two-dimensional body, for example a circular cylinder[3-1),3-2)]. Further, in general there are still very few studies on the characteristics of the pdf profiles of passive scalar concentration fields[3-3)~3-8)]. In such situation, to elucidate the diffusion mechanism around the body, it is important and necessary to examine more in detail the characteristics of concentration pdf (for example, see references 3-7) and 3-8)). The research reported in this chapter was made taking account the above scientific requirements.

Nomenclature of chapter 3

x, y, z	:	mean streamwise, horizontal and vertical coordinates (see Fig. 2.1)
r, θ, ϕ	:	coordinates in the sphere frame (see Fig. 2.1)
U_0	:	mean velocity of main stream
Γ_j	:	initial concentration at the nozzle exit
Γ, γ'	:	conventional mean concentration and concentration fluctuation rms value
$\langle\Gamma\rangle, \langle\gamma'\rangle$	:	conditional mean concentration and concentration fluctuation rms value
S_k, S_k^*	:	conventional and conditional skewness factor of concentration fluctuation signal
F_L, F_L^*	:	conventional and conditional flatness factor of concentration fluctuation signal
f, f^*	:	conventional and conditional pdf of concentration
D	:	molecular diffusivity (m^2/sec)
ω_Γ	:	concentration detecting frequency
d, a	:	diameter and radius of the sphere
C_Γ	:	spatial concentration correlation coefficient
$\hat{C}_\Gamma$	:	temporal auto-correlation coefficient of concentration at one spatial point
L_Γ, λ_Γ	:	integral and dissipation length scale for concentration field

superscript
~ : instantaneous value
other notations will be defined each time

3. 2 Distortion of material lump due to a sphere

As shown in Figs. 2.6 and 2.7, a large distortion of mean flow field occurs near the stagnation point. Here, we will consider how the size of a material lump changes along the stagnation stream line by such a distortion of mean flow field (see Fig. 3.1). Supposing a material lump has its streamwise size of d_0 at some point upstream the stagnation point at the time $t=0$, the size of this lump after the time t will be estimated as follows,

$$d_t = d_0 exp(-\alpha t) \tag{3.1}$$

where α means the non-dimensional compression rate ($= |(\partial U/\partial x)(d/U_0)|$) and that is supposed to be constant.

Since in the actual mean flow field α is a function of the position on the stagnation line, we should take the Lagrangian integration along the pass of fluid particle as follows,

$$d_t = d_0 exp\left\{-\int_0^t \alpha(t')dt'\right\}. \tag{3.2}$$

Now as the starting position of lump, we chose the location where the mean flow begins to have the distortion effect due to a sphere (here we chose $(x+a)/d=-1$, $x=-90$ mm). In this case, d_0 represents the streamwise length scale of the material lump at $x=-90$ mm. Fig. 3.1 shows the change of d_t as the lump approaches to the stagnation point in each case of

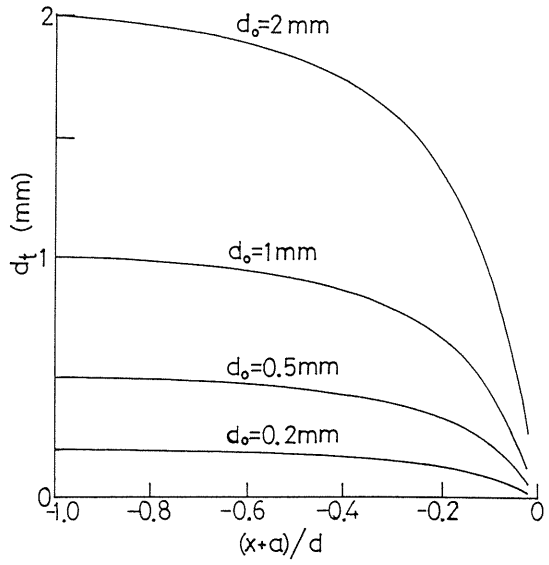

Fig. 3.1 Change of size of substance lump by the mean flow distortion.

d_0 = 2,1,0.5,0.2 mm. From the figure, it is found that d_t becomes about 0.27 mm at $x = -31$ mm ($(x+a)/d = -0.017$) in case of $d_0 = 2$ mm. As referring to later, the integral length scale of the concentration field shows almost constant value at the far downstream region from the stagnation point, and its value is about 2 mm. This means that the integral length scale of lump at the upstream region will be distorted to about 0.27 mm on average in the vicinity of the stagnation point. Subsequently, considering only the effect of mean flow distortion it can be expected that the change of concentration in the integral length scale of lump at the upstream region can be detected by the present micro-fiber probe of core diameter 100 μm even at the region very close to the stagnation point such as $x = -31$ mm. However, in case of $d_0 = 0.5$ mm, d_t becomes about 0.063 mm at $x = -31$ mm. So it becomes impossible to detect the change of this scale of structure at $x = -31$ mm by the present probe. And further it is noted that since this kind of distortion of the flow field the coalescence of the material lines occurs in accompany with the progress of molecular diffusion, so that the smeariness will increase (see references 3-10) and 3-11)).

3. 3 On the method of conditional analysis for the concentration data

There are two useful methods, i.e. Gaussian Fitting method and Threshold Level method[3-3),3-10),3-12)], to obtain the intermittency factor and conditional pdf. Here we note that these two methods are closely connected with each other. Although we can choose the most suitable value by examining the dependency of the concentration detecting frequency on the threshold, here the threshold was determined by the following equation according to the reference 3-12),

$$TH = E_0 + 1.5\sigma_n, \tag{3.3}$$

where E_0 is the output voltage of the measuring circuit when $\tilde{\Gamma} = 0$ and σ_n denotes the standard deviation of noise. We ascertained that the intermittency factor calculated by using the above threshold show a good agreement with one by the Gaussian Fitting method.

3. 4 Experimental results and discussions

As shown in section 3.2, the large distortion of the flow field occurs in particular near the stagnation point. We can expect that such distortion gives a remarkable effect on the internal structure of the diffusing plume.

The downstream change of the concentration detecting frequency ω_Γ on the stagnation line is shown in Fig. 3.2, where the ordinate is non-dimensionalized by using the local mean velocity U and the diameter of sphere d. The concentration detecting frequency ω_Γ is defined as follows.

$$\omega_\Gamma = \textit{the number of times that the measuring probe detects the concentration field per unit time period (one second)} \tag{3.4}$$

Whe we define N_{th} as the number of points of intersection between the threshold line and the concentration signal, ω_Γ can be expressed by

$$\omega_\Gamma = (N_{th}/2)/T, \tag{3.5}$$

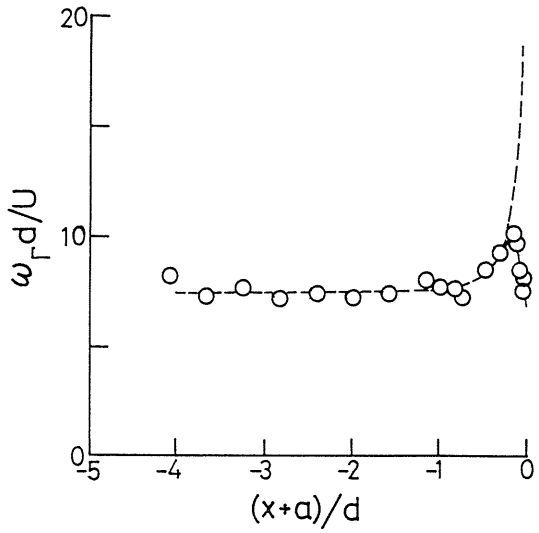

Fig. 3.2 Change of the concentration detecting frequency on the stagnation line.

where T is the time period of measurement. It is here noted that so as to non-dimensionalize ω_Γ we chose the local velocity U as the reference velocity instead of the main stream velocity U_0. This selection is useful to extract the change of spatial structure of the diffusing plume explicitly (practically if we use U_0 as the reference velocity, the non-dimensionalized concentration detecting frequency shows the monotonous decrease downstream along the stagnation line so that we can not see explicitly any change of the spatial structure of diffusing plume). As found from Fig. 3.2, at the far region from the sphere the non-dimensionalized concentration detecting frequency shows almost constant value. However as the sphere is approached at the region downstream from $(x+a)/d=-1$, that increase gradually and takes the peak at some position near the stagnation point ($(x+a)/d \sim 0.20$), then decreases rapidly. The above change of non-dimensionalized concentration detecting frequency can be understood as follows. At first, from the position $(x+a)/d=-1$, the structure of the plume begins to be compressed by the effect of distortion of mean velocity field (here we call it "the direct effect of distortion"). The compression of the plume structure causes the increase of the non-dimensionalized concentration detecting frequency. This phenomenon can be explained by the following sample model. Now we suppose the material striae at the far upstream region from the stagnation point. Since the trajectory of fluid particle can be calculated by integrating the mean velocity field, we can easily estimate the change of the non-dimensionalized concentration detecting frequency caused only by the distortion effect of the mean velocity field. Its result is the broken line in Fig. 3.2, and that shows definitely monotonous increase as the sphere is approached. On the other hand, we can expect naturally the effect of the change of turbulence structure by the distortion (we call this effect "the indirect effect of distortion"). However, as shown in Fig. 3.2, the calculation result agrees very well with the experimental data until the x position where the non-dimensionalized concentration detecting frequency takes the peak value. This means that the direct effect of distortion is more dominant on the change of detecting frequency than the indirect effect of distortion. Next as the sphere is approaching more, the coalescence of the material lumps (or layers, lines[3-10),3-13)]) occurs, and further even though such coalescence does not come about, the present probe

can not discriminate between two lumps if the gap between two lumps become less than 0.3 mm. The compression of the flow field and the above situation may lead to the rapid decreasing of the non-dimensionalized concentration detecting frequency very near the stagnation point. Figs. 3.3(a) ~ (c) show the radial changes of the conventional pdf profile around

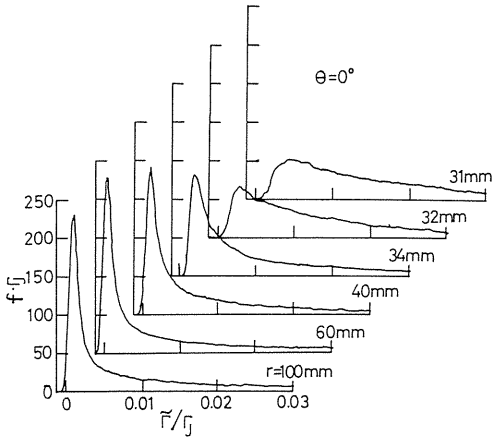

Fig. 3.3 (a) Change of conventional pdf profile of concentration on the stagnation line.

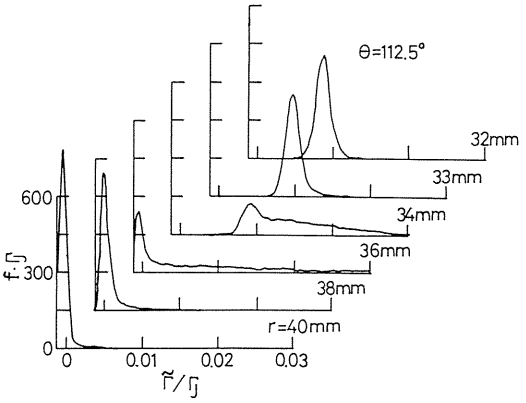

Fig. 3.3 (b) Radial change of conventional pdf profile of concentration at $\theta = 112.5°$.

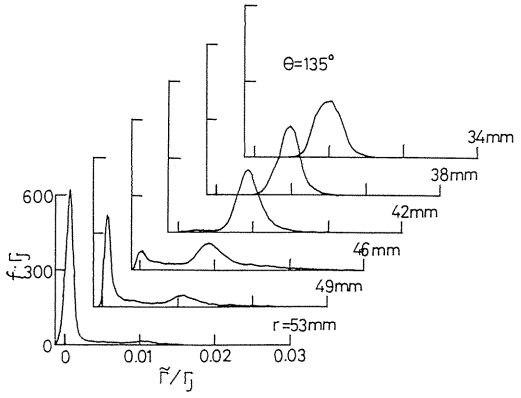

Fig. 3.3 (c) Radial change of conventional pdf profile of concentration at $\theta = 135°$.

the sphere. On the stagnation line of $\theta = 0°$, the height of the spike at $\tilde{\Gamma} = 0$ fall down and its position move to the higher positive concentration as the sphere is approached. This phenomenon can be understood in terms of the increase of smeariness caused by the coalescence of the material lumps by the molecular diffusion. Further, from the figure it is found that at $\theta = 112.5°$ and 135°, the conventional pdf profile shows different characteristics in each region i.e. recirculating wake region, separated shear layer and outside the recirculating wake region. At first, in the recirculating wake region, the diffusing matter tends to stay there in particular in neighborhood of the wall in the long time, so that the molecular diffusion makes fairly progress and the conventional pdf becomes lognormal[3-8),3-11)]. On the other hand, outside the recirculating wake region, the diffusing plume becomes so intermittent that the conventional pdf becomes to have a peak near $\tilde{\Gamma} = 0$, and shows a very small value in other concentration region. The above characteristics of pdf profile are known to be typical for the intermittent phenomena. Further, in and around the separated shear layer, there exists the strong vortical motion which entrains not only the concentration structure in the recirculating wake region where the molecular diffusion has fairly advanced but also the intermittent plume outside the recirculating wake region. Consequently, the conventional pdf in the separated shear layer shows the combined characteristics inside and outside the recirculating wake region, i.e. the double-peaks profile. In particular we can observe clearly such characteristics at $\theta = 135°$.

The change of conventional and conditional skewness factor of concentration signal S_k, S_k^* are shown in Fig. 3.4, where S_k and S_k^* are defined by

$$S_k = \frac{\int_0^\infty (\tilde{\Gamma} - \Gamma)^3 f(\tilde{\Gamma}) d\tilde{\Gamma}}{\gamma'^3} \tag{3.6}$$

$$S_k^* = \frac{\int_0^\infty (\tilde{\Gamma} - \Gamma)^3 f^*(\tilde{\Gamma}) d\tilde{\Gamma}}{\langle \gamma' \rangle^3} \tag{3.7}$$

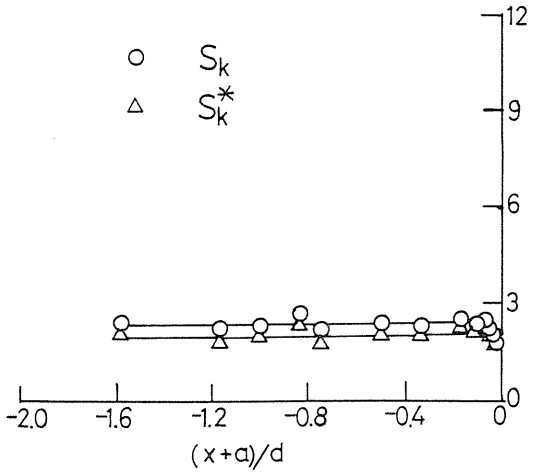

Fig. 3.4 Distribution of conventional and conditional skewness factor on the stagnation line.

At the far region from the sphere, S_k and S_k^* keep almost constant values. Near the stagnation point, these are rapidly decreasing as the sphere is approached. The above result can be supposed from the changes of conventional pdf (in Fig. 5.3(a)) and conditional pdf (in reference 3-10)).

Figure 3.5 gives the changes of conventional flatness factor F_L and conditional flatness factor F_L^* on the stagnation line. F_L and F_L^* are defined by

$$F_L = \frac{\int_0^\infty (\tilde{\Gamma} - \Gamma)^4 f(\tilde{\Gamma}) d\tilde{\Gamma}}{\gamma'^4} \tag{3.8}$$

$$F_L^* = \frac{\int_0^\infty (\tilde{\Gamma} - \Gamma)^4 f^*(\tilde{\Gamma}) d\tilde{\Gamma}}{\langle \gamma' \rangle^4} . \tag{3.9}$$

In the same way as S_k and S_k^*, it is also obvious that F_L and F_L^* take almost constant value at the far region from the sphere, and decrease near the stagnation point. Such changes of F_L and F_L^* are not inconsistent with changes of conventional and conditional pdf of concentration signal. Fig. 3.6 shows the radial distribution of S_k around the sphere except $\theta = 0°$. At $\theta < 112.5°$, S_k increases as the position departs from the sphere. On the other hand, At $\theta \geq 112.5°$, (in the separate flow region) we can observe very interesting change of S_k. At first, in the vicinity of the wall, S_k shows the small value but not zero (order of 1.0), so that we can conclude that the conventional pdf of concentration here is not a symmetric Gaussian distribution. In fact, it has been already ascertained by authors[3-11] that the conventional pdf in the vicinity of the wall shows the lognormal distribution. Next, at a little way off from the sphere, a high level of concentration layer which is not diluted so much by the molecular diffusion yet comes sometimes to the measuring point. Eventually, the conventional pdf distribution becomes to deviate from lognormal distribution so that the right hand side of lognormal distribution swells up like the distribution at $r = 34$ mm in Fig. 3.3(b) ($\theta = 112.5°$).

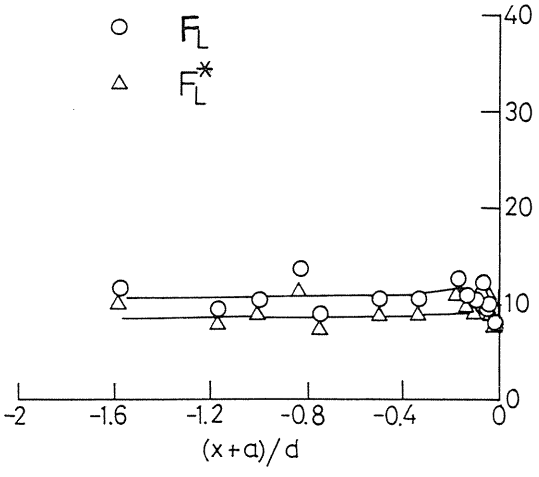

Fig. 3.5 Distribution of conventional and conditional flatness factor on the stagnation line.

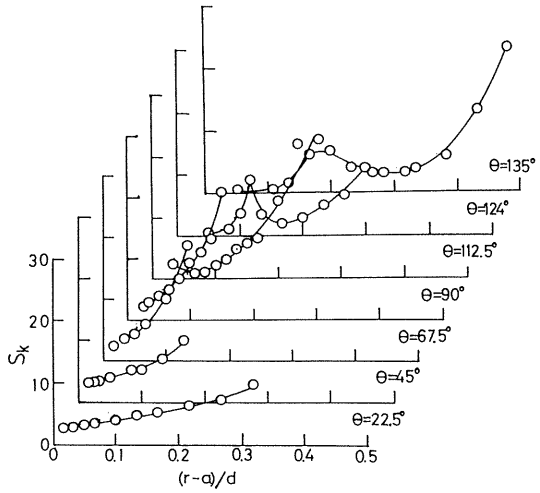

Fig. 3.6 Radial change of conventional skewness factor for the concentration field at each θ.

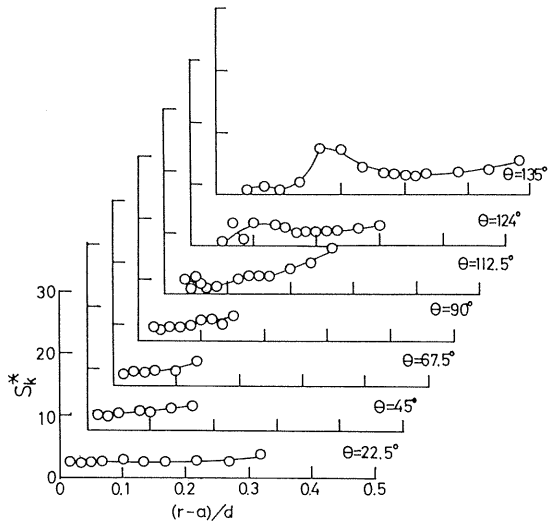

Fig. 3.7 Radial change of conditional skewness factor for the concentration field at each θ.

However, if the measuring point enters into the separated shear layer apart from the sphere, a plume having a high conditional concentration come to the measuring point intermittently from the outside, so that the conventional pdf distribution becomes to have double-peaks like ones explained before. At that time, since the peak which appears near $\tilde{\Gamma} = 0$ becomes to balance with a lognormal bulge at $\tilde{\Gamma} \neq 0$, conventional skewness factor will decrease again. At the outside of the separated layer, the plume is highly intermittent and the large spike near $\tilde{\Gamma} = 0$ appears in the conventional pdf distribution. Naturally we observe a very high value of S_k^* at the outside of the separated layer.

Figure 3.7 gives the radial distributions of S_k^* around the sphere except $\theta = 0°$.

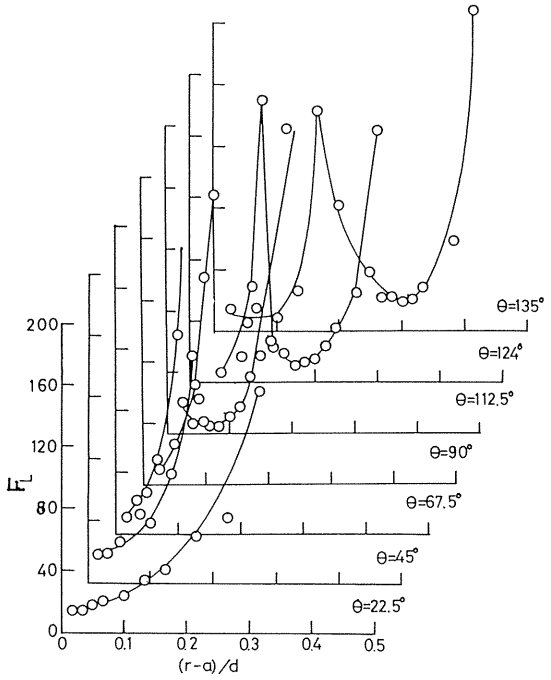

Fig. 3.8 Radial change of conventional flatness factor for the concentration field at each θ.

It is obvious that the radial change of S_k^* is much smaller compared with one of S_k. Further, we can also observe the distributions of S_k^* is similar to ones of S_k at $\theta \geq 112.5°$.

Figure 3.8 shows the distribution of F_L at each value of θ except on the stagnation line. At $\theta < 112.5°$, F_L goes up as the position departs from the sphere. On the other hand, at $\theta \geq 112.5°$, the radial changes of F_L are very similar to ones of conventional skewness factor S_k.

The radial distributions of F_L^* at each value of θ are given in Fig. 3.9. From the figure, it is clear that at $\theta < 112.5°$ the change of F_L^* is much smaller than the change of F_L. At $\theta \geq 112.5°$, F_L^* shows the very similar radial change to F_L.

On the stagnation line, the effect of the distortion of the flow appears also clearly on the distribution of concentration auto-correlation coefficient.

The change of the concentration correlation coefficient $C_\Gamma(\xi)$ for two spatially separate points located on the stagnation line is shown in Fig. 3.10, where $C_\Gamma(\xi)$ is obtained by using the Taylor's hypothesis of frozen pattern in the following. At first we introduce the auto-correlation coefficient $\hat{C}_\Gamma$ for the concentration fluctuation signal with the time delay τ at a fixed spatial point, which is defined by

$$\hat{C}_\Gamma(\tau) = \frac{\overline{\{\tilde{\Gamma}(x', t) - \Gamma\}\{\tilde{\Gamma}(x', t+\tau) - \Gamma\}}}{\overline{\{\tilde{\Gamma}(x', t) - \Gamma\}^2}} \tag{3.10}$$

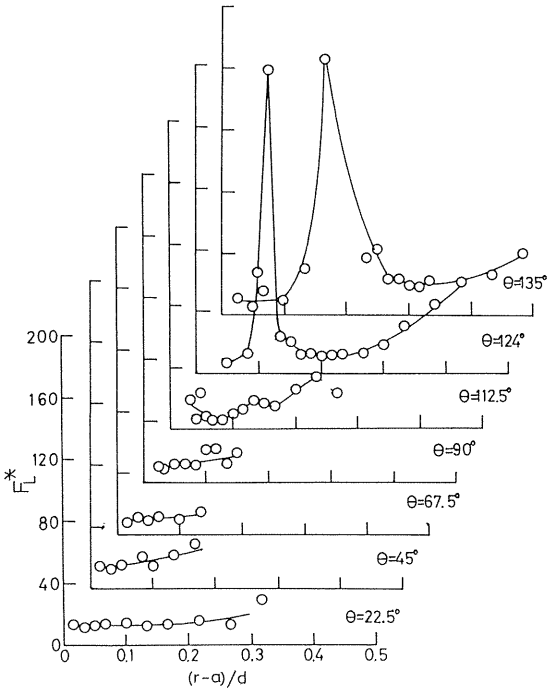

Fig. 3.9 Radial change of conditional flatness factor for the concentration field at each θ.

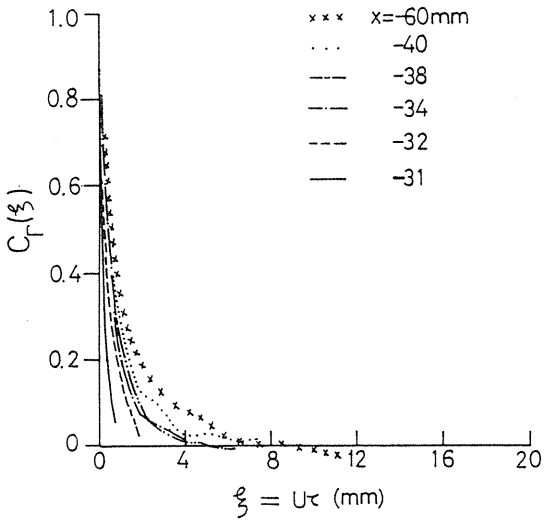

Fig. 3.10 Change of two point correlation coefficient for the concentration field on the stagnation line.

The Taylor's hypothesis of frozen pattern of concentration field can be expressed by

$$\tilde{\Gamma}(x', t + \tau) = \tilde{\Gamma}(x' - U\tau, t). \tag{3.11}$$

Then we obtain

$$\begin{aligned}\tilde{\Gamma}(x', t)\tilde{\Gamma}(x', t + \tau) &= \tilde{\Gamma}(x', t)\tilde{\Gamma}(x' - U\tau, t) \\ &= \tilde{\Gamma}(x')\tilde{\Gamma}(x' - U\tau).\end{aligned} \tag{3.12}$$

Considering Eqs. (3.11) and (3.12), Eq. (3.10) can be rewritten as follows,

$$\begin{aligned}\hat{C}_\Gamma(\tau) &= \frac{\overline{\{\tilde{\Gamma}(x') - \Gamma\}\{\tilde{\Gamma}(x' - U\tau) - \Gamma\}}}{\overline{\{\tilde{\Gamma}(x') - \Gamma\}^2}} \\ &= \hat{C}_\Gamma(-U\tau) = C_\Gamma(U\tau)\end{aligned} \tag{3.13}$$

where $C_\Gamma(\xi)$ is the spatial correlation coefficient for the two points with the streamwise distance $\xi = U\tau$. In Fig. 3.10, the product of the local mean velocity U and the time difference τ is taken as the abscissa. Since it was ascertained by the experiments that the relative intensity of turbulence is enough small except $x = -31$ mm (see chapter 2 and references 3-10), 3-11) and 3-14)), the Taylor's hypothesis is approximately true and $U\tau$ may be regarded as the spatial distance for the two point correlation coefficient. From this figure it can be observed that as the stagnation point is approached the extent and magnitude of correlation coefficient are reduced, and this tendency becomes quick in particular near the stagnation point. From the concentration correlation coefficient, the integral length scale of concentration field can be calculated by

$$L_\Gamma = \int_0^\infty C_\Gamma(\xi) d\xi. \tag{3.14}$$

The change of L_Γ on the stagnation line is given in Fig. 3.11. In the same figure, the dissipation scale of concentration field λ_Γ is also shown. λ_Γ can be here calculated from the following equation,

$$\frac{1}{\lambda_\Gamma^2} = \frac{\overline{(\partial\tilde{\Gamma}/\partial t)^2}}{2\gamma'^2 U^2}, \tag{3.15}$$

where Taylor's hypothesis is also used. As shown in Fig. 3.11, both L_Γ and λ_Γ decrease rapidly near the stagnation point.

From Fig. 3.11, the ratio of L_Γ to λ_Γ can be easily calculated and its change on the stagnation line is given in Fig. 3.12. As found in Fig. 3.12, at the region far away from the sphere, L_Γ/λ_Γ shows the almost constant value, but it decreases rapidly near the stagnation point. This means that the reduction of L_Γ by the flow distortion is much larger than one of λ_Γ near the stagnation point. This phenomenon may be caused by the coalescence of the diffusing lumps[3-10] which received large distortion, because by the coalescence the concentra-

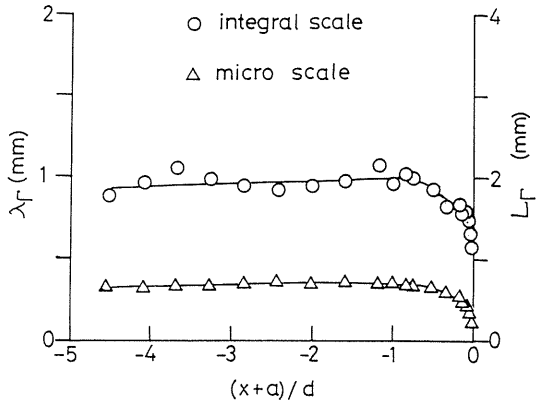

Fig. 3.11 Changes of integral and dissipation length scale for the concentration field on the stagnation line.

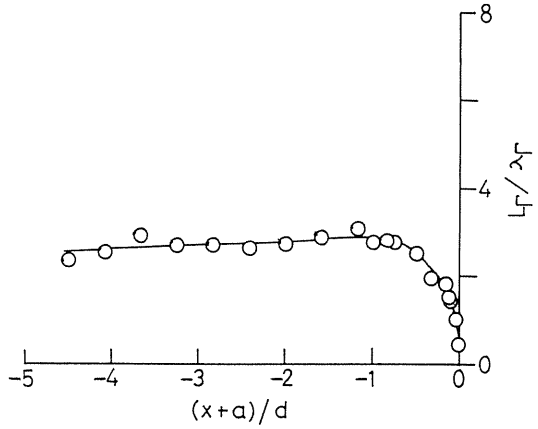

Fig. 3.12 Change of ratio of integral length scale to dissipation length scale for the concentration field on the stagnation line.

tion structure of small scale is much reduced while the effect of such coalescence on the integral scale can be expected to be relatively small.

From results in this chapter and references 3-10) and 3-11), we can suggest two important effects of the flow distortion on the change of concentration structure near the stagnation point as schematically shown in Fig. 3.13(a) and (b). At first, by the distortion of mean velocity field the material lumps (like layer or line) are compressed in the x direction and become slim. This compression effect by the distortion of the flow (we call it 'the first effect') is shown in Fig. 3.13(a). On the other hand, at the same time that the material lumps becomes slim, the gaps between them are also reduced. Consequently, the merging of material lumps (we call it 'the second effect' or 'smeariness effect'[3-10]) occurs, as shown in Fig. 3.13(b). In actuality, we expect that the above two effects synthetically bring about the

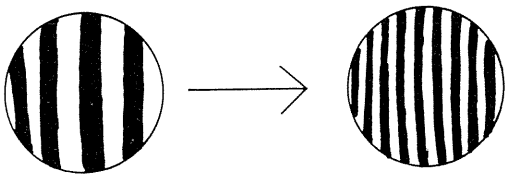

(a) Compression effect by the distortion

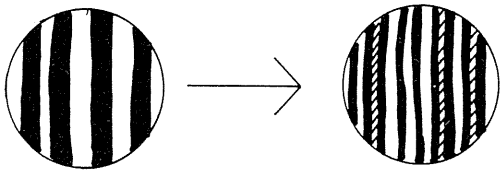

(b) Smeariness effect by the molecular diffusion

Fig. 3.13 Effects of flow distortion on the structure of diffusion field.

change of the structure of a diffusing plume. It is noticed that although we can also consider the indirect effect by the flow distortion i.e. the change of turbulence, this effect is quite small in comparison with the direct effect like compression by the flow distortion, as explained for Fig. 3.2.

Here it is of necessity to give some comments on the influences of the probe resolution and molecular diffusion on the results by data-analysis in this study. Although the limitation of resolution of the probe hinders the clear understanding of the effect of molecular diffusion, we will here try to make some specific estimation of the effect of molecular diffusion by using the same calculation as § 3.2. If we set the material lump with the size of $d_0 \sim 0.2$ mm at $x = -90$ mm, which is the same order of the resolution of the probe, the size of lump becomes about 0.025 mm at $x = -31$ mm by the distortion of the mean flow (see Fig. 3.1). On the other hand, the broadening length of the edge of lump by the molecular diffusion can be estimated as $(2D\Delta t)^{1/2} \simeq [2 \times \{1.307 \times 10^{-6}/(4 \times 10^{3})\} \times 60/129]^{1/2} \simeq 0.0175$ mm, where Δt is the moving time of fluid particle by the mean velocity from $x = -90$ mm to $x = -31$ mm, i.e. $\Delta t \simeq d/U_0 = 60/129$. Since the molecular diffusion progresses into both side of the space between the neighboring lumps, the length filled up by the molecular diffusion is 2×0.175 mm $= 0.035$ mm. This length is clearly larger than the above distorted size of lump 0.025 mm at $x = -31$ mm. So there is a good possibility that the gap between neighboring lumps is completely filed up only by the molecular diffusion.

3. 5 Conclusions

The conventional and conditional statistics regarding the pdf of concentration fluctuation are investigated in detail for the axisymmetric point-source plume which develops in the turbulent flow distorted by the sphere. The results obtained in this chapter are summarized as follows.

On the upstream stagnation line, the non-dimensionalized concentration detecting frequency $\omega_\Gamma d/U$ shows almost constant value far away from the sphere. As the sphere is approached on the stagnation line, $\omega_\Gamma d/U$ begins to increase from the position of $(x+a)/d \sim -1$ mainly because of the effect of the mean flow distortion due to the sphere, takes the peak, then changes to rapid decrease in the vincinity of the stagnation point (at $(x+a)/d \leq -0.2$).

The ratio of the integral length scale to the dissipation length scale for the concentration field on the stagnation line shows the rapid decrease near the stagnation point as the sphere is approached. Further, with regard to the skewness and flatness factor, the conventional values gives all the rapid decrease near the stagnation point. On the other hand, at the downstream region from the separation point of the flow the radial distributions of the conventional and conditional values of skewness and flatness factor present a different tendency from ones on the stagnation line. As the position moves apart from the sphere, they all show the increase at first, and take the maximum inside of the separated shear layer. Outside of shear layer, they fall down once, and then increase again.

References of chapter 3

3-1) Tsunoda, H., Sakai, Y. and Nakamura, I., "The disturbance effect of a circular cylinder on the diffusion of matter by a plume from a point source in grid-generated turbulence (3rd report, Characteristics of the conditional statistics)", *Trans. JSME.,* Vol.54, No.503 (1988), 1581, (in Japanese).

3-2) Tsunoda, H., Sakai, Y., Nakamura, I. and Liu, S., "The effect of a circular cylinder on the diffusion of matter by a plume", *J. Fluid Mech.* (1993), Vol.246, 419.

3-3) Bilger, R.W., Antonia, R.A. and Sreenivasan, K.R., "Determination of intermittency from the probability density function of a passive scalar", *Phys. Fluids,* Vol.19, No.10 (1976), 1471.

3-4) Tsunoda, H., "Experimental study on the continuous point source plume in the shear flows", *ph.D. Dissertation* (1988), Nagoya University, Japan, (in Japanese).

3-5) Pope S.B., "Pdf methods for turbulent reactive flows" *Prog. Energy Combust. Sci.,* Vol.11 (1985), 119.

3-6) Sakai, Y., "Experimental study on the diffusion by the light absorption method", *ph.D. Dissertation* (1984), Nagoya University, Japan, (in Japanese).

3-7) O'Brien, E.E., "Stochastic properties of scalar quantities advected by a non-buoyant plume", *J. Fluid Mech.,* Vol.89, part 2 (1978), 209.

3-8) Csanady, G.T., *Turbulent Diffusion in the Environment, Geophysics and Astrophysics Monographs, Vol.3,* D. Reidel Publishing Company (1973), 222.

3-9) Hinze, J.O., *Turbulence, 2nd Edition,* McGraw-Hill (1975), 413.

3-10) Liu, S., Tsunoda, H., Sakai, Y. and Nakamura, I., "Stochastic characteristics of a point-source plume diffusion field upstream of sphere", *Trans. JSME.,* Vol.57, No.541 (1991), 2976, (in Japanese).

3-11) Sakai, Y., Liu, S., Tsunoda, H. and Nakamura, I., "On the statistics of a point-source plume around a sphere", *Trans. JSME.,* Vol.58, No.545 (1992), 51, (in Japanese).

3-12) Nakamura, I., Sakai, Y. and Tsunoda, H., "On the conditional statistics of the diffusion field of matter by a point source plume in uniform mean shear flow", *JSME. Int. J.,* Series II, Vol.32, No.2 (1989), 180.

3-13) Ottino, J.M., *The Kinematics of Mixing, Stretching, Chaos and Transport,* Cambridge University Press (1989), 1.

3-14) Nakamura, I., Sakai, Y. Tsunoda, H. and Liu, S., "On the effect of disturbance of a sphere on the point source diffusion process in grid-generated turbulence", *Proc. of 7th Symposium on Turbulent Shear Flows* (1989), Stanford University, 14.5.1.

4. Fractal Feature of a Diffusing Plume and Effects of the Distortion of Flow due to a Sphere

4. 1 Introduction

So as to experimentally clarify the effect of the distortion of flow due to a sphere on the axisymmetric point source diffusing plume, we have carried out detailed investigations on the elementary statistical characteristics of the flow and the diffusion field so far (see chapters 2, 3 and references 4-1), 4-2)). In this chapter, we apply the fractal analysis, which has been rapidly developed to study scalar diffusions, to reveal the stochastic structure of the plume.

Since the concept of *fractal* was first proposed by Mandelbrot[4-3)], several years elapsed and the study of fractal has become a global subject, together with that of chaos. Particularly, the fractal study in hydrodynamics aspect has become increasingly active. In the light of these works, it is revealed that a variety of fractalities involved in turbulence. For example, the turbulence-nonturbulence interface in boundary layers[4-4)] and the iso-concentration surface in passive scalar diffusion field[4-5)] have been shown to be fractal-like by many researchers. So are the interfaces generated by Kelvin-Helmholz instability and the surfaces of clouds[4-6)] in the atmosphere. The common feature of these surfaces is that their fractal dimensions are almost the same, i.e. $D = 2.36 \pm 0.05$[4-5)]. However, there is no investigation on the fractality of passive scalar plumes such as we have been studying, despite of its fundamental significance. So, we attempt to reveal the fractality of the point source diffusing plume evolved in the grid-generated turbulence by analyzing the data of concentration sampled with our own optical fiber probe (see section 2.2 in chapter 2). Furthermore, we are going to clarify the effect of the distortion of flow due to a sphere on the fractality of the diffusing plume. In the consequent sections, the results of our analysis and brief discussions will be given.

Nomenclature of chapter 4

x, y, z	:	main streamwise, horizontal and vertical coordinates (see Fig. 2.1)
r, θ, ϕ	:	coordinates in the spherical frame (see Fig. 2.1).
U_0, u'	:	mean velocity of the main stream and the velocity fluctuation rms value.
Γ, γ'	:	conventional mean concentration and concentration fluctuation rms value.
$\langle\Gamma\rangle, \langle\gamma\rangle$	:	conditional mean concentration and concentration fluctuation rms value.
ν	:	kinematic viscosity of water.
D_f	:	fractal dimension.
η	:	Kolmogorov scale.
d, a	:	diameter and radius of the sphere.
L_Γ, λ_Γ	:	integral length scale and dissipation scale of the concentration field.
TH	:	threshold level.

Other notions are interpreted as they appear.

4. 2 Kolmogorov length scale and the resolution of the probe

The experimental setup and flow outline were explained in detail in chapter 2. Here mainly discussed is the relationship between the Kolmogorov length scale and spatial resolution of fiber probe.

We could estimate the Kolmogorov scale of the flow as follows.

$$\eta = (\nu^3/\varepsilon)^{1/4}, \tag{4.1}$$

where ε expresses the dissipation rate of kinematic energy of the turbulence, and may be calculated from equation (4.2)[4-7].

$$\varepsilon \sim -(3/2)U_0 d(u')^2/dx, \tag{4.2}$$

The magnitude of ε could be calculated using equations (4.1) and (4.2), but we have to account that ε should be dependent on the relative position respect to the sphere. If we focus on the area free of the disturbance of the sphere, i.e. $x = -250 \sim -90$ mm, η could be shown to be 1 mm or so. The resolution of the probe we used is 0.31 mm, and it is about 1/3 of the magnitude of η, so this probe is able to recognize the sub-Kolmogorov scale structures of the diffusing plume. It should be noted that the Schmidt number of the dye solution is about 3.8×10^3, and the so-called Batchelor scale of the diffusion field is estimated as $\eta_b = \eta Sc^{-1/2} \approx \eta/60$. Consequently, although this probe is able to recognize the sub-Kolmogorov scale structures, it is not able to recognize the structure in the *B range*, which was named by Prasad & Sreenivasan[4-9]. In another word, it is only able to catch a fraction of the structures in the range between the Kolmogorov scale and the Batchelor scale. Note, this probe is expected to be sufficiently resolutive to catch the structures within the range between the Kolmogorov scale and the integral length scale, the so-called *K range*[4-8]. For more details on the flow, see chapter 2.

It is worthwhile considering the physical meaning of the signal measured by the optical fiber probe. As motioned above, the sampling volume of this probe could be taken as the cylindrical passage of the laser beam between two fibers. In our case, the diameter of this cylindrical passage d_L is 100 μm, and the length $L_p \approx 0.31$ mm. Because L_p is much larger than d_L in this case, we only consider the effect of L_p. Consider the probe frame shown in Fig. 4.1. We could then write the instantaneous concentration $\tilde{\Gamma}_{Lp}(t)$ as the following integration over the sampling volume.

$$\begin{aligned}\tilde{\Gamma}_{Lp} &= \frac{1}{AL_p}\int dx_p \int dz_p \int_0^{Lp} \tilde{\Gamma}(x_p, y_p, z_p, t)\, dy_p \\ &= \frac{1}{AL_p}\int_0^{Lp} \left[\int \int \tilde{\Gamma}(x_p, y_p, z_p, t)\, dx_p dz_p\right] dy_p \\ &= \frac{1}{L_p}\int_0^{Lp} \tilde{\Gamma}(y_p, t)\, dy_p,\end{aligned} \tag{4.3}$$

where the integration of x_p and z_p are only operated within the cross-sections of the cylindrical passage of laser beam, which is expressed by A in the equation, and $\tilde{\Gamma}(x_p, y_p, z_p, t)$ denotes the instantaneous concentration at any point of space. Note that we have used the notion that the beam intensity is proportional to the cross area of the passage and the Lambert-Beer law in the derivation of equation (4.3). $\Gamma'(y_p, t)$ in the above equation is the average concentration over the cross-section of beam, which is defined as follows.

$$\Gamma'(y_p, t) = \frac{1}{A}\int \int \tilde{\Gamma}(x_p, y_p, z_p, t)\, dx_p dz_p \tag{4.4}$$

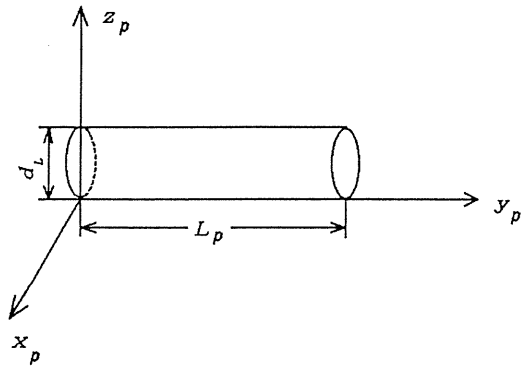

Fig. 4.1 Model of sample volume by the fiber probe.

From equations (4.3) and (4.4), we could see that the signal of the probe is only the integral average of $\Gamma'(y_p,t)$ over the length of the sampling volume. This means that what we get with this probe is approximately the overlapped version of all the diffusion structures in the planes whose normals are in parallel with the beam passing through the sampling volume. If we compare our case with the laser sheet method with LIF used by Prasad et al.[4-8], L_p may correspond to the thickness of laser sheet.

4. 3 Algorithm of fractal analysis

The scheme we adapted for the determination of the fractal dimension is the so-called box-counting algorithm[4-3),4-9),4-10)], which divides the E-dimensional space into cubic elements sized ε, and plots the number of the cubes involving the focused object, $N(\varepsilon)$, against ε, and give the slope of the $N(\varepsilon) \sim \varepsilon$, which is directly related to the fractal dimension of the object. If the object is a fractal, then we have the following relation.

$$N(\varepsilon) \sim \varepsilon^{-D_{fE}}, \tag{4.5}$$

where the subscript E in D_{fE} means the E-dimensional Euclidian space.

In this study, we dealt with the set of iso-concentration points which is shown in Fig. 4.2 (a) and (b). The unit pulses shown in Fig. 4.2 (b) are generated at the intersecting points between the iso-concentration threshold line and the concentration signal. The experimental data analyzed here are the discrete time series which are obtained by the A-D transformation (sampling frequency is 5000 Hz) of the analogue concentration signal measured at the fixed spatial point. Since at the region far from the sphere the mean velocity is much larger than the turbulent fluctuation, the Taylor's hypothesis of the frozen turbulence seems to be approximately true, i.e., the spatial structure of the diffusing plume is almost directly reflected on the time series measured at the fixed point. Then the series of the unit pulse correspond to the one-dimensional interesting points between the iso-concentration surface (which exists if the concentration field is continuous) and the straight line. Since the actual iso-concentration surface is embedded in the three-dimensional space, its dimension D_{f3} can be estimated by [4-3),4-5)]

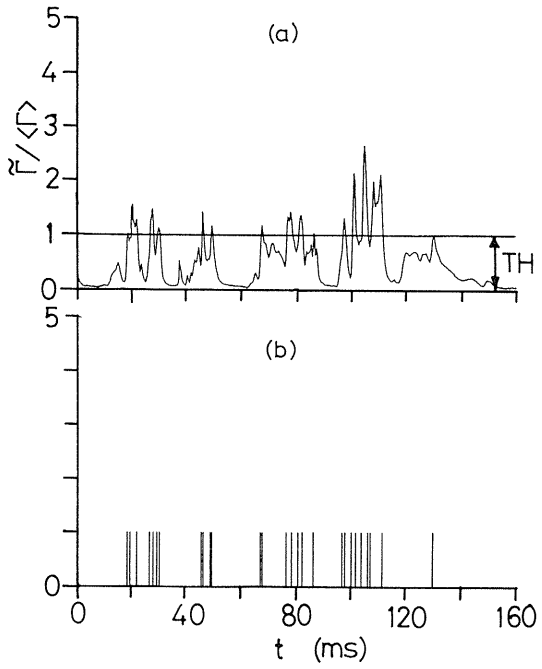

Fig. 4.2 Examples of the concentration signal and a set of iso-concentration points.
(a): Concentration signal.
(b): Set of iso-concentration points.

$$D_{f3} = D_{f1} + 2. \tag{4.6}$$

To compare our results with other studies, the fractal dimension of the iso-concentration surface reported here is always the value of D_{f3} which was calculated by the above equation (4.6) from the measured one-dimensional dimension D_{f1}. When estimating the fractal dimension from the curve of $\ln N(\varepsilon)$ vs. $\ln \varepsilon$, it is important to decide the region of the size of ε in which the constant slope of $\ln N(\varepsilon)$ vs. $\ln \varepsilon$ can be observed. Although there is no established way to decide this constant slope region, as one trial in this study, from the observation of the actual curve of $\ln N(\varepsilon)$ vs. $\ln \varepsilon$, the integral length scale of the concentration field L_Γ was chosen as the maximum of the constant slope region, and the diameter of the laser beam (about 0.1 mm) passing though the gap between two glass fibers as the minimum of this region. As shown later, we can observe the good linear relation between $\ln N(\varepsilon)$ and $\ln \varepsilon$ at $d_L \leq \varepsilon \leq L_\Gamma$ notwithstanding the change of the threshold, so that we want to emphasize the fractal dimension computed in the region of ε over the probe's spatial resolution L_p could be accurately determined in the present study. Another important factor to compute the fractal dimension is the data segment length. We investigated the effect of the data segment length on the fractal dimension, so that it was confirmed that if the data segment length for computing the dimension is larger than the ten times of the integral length scale of the concentration field L_Γ, the fractal dimension does not depend on the data segment length, as shown in Figs. 4.3 and 4.4. In Fig. 4.3, the parameter SI indicates the number of data included in one

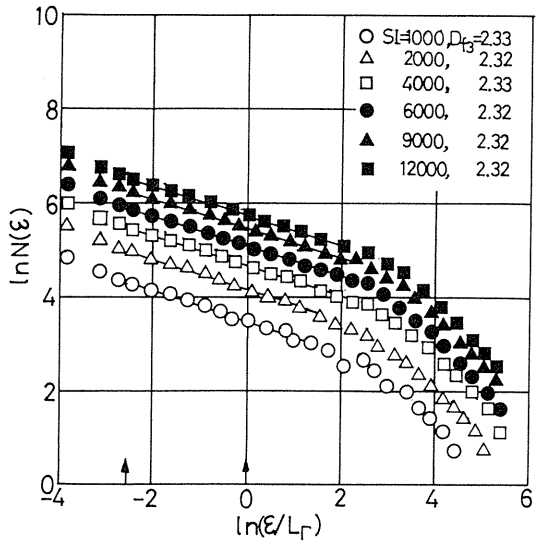

Fig. 4.3 Effect of the data segment length on the curve of $\ln N(\varepsilon)$ vs. $\ln \varepsilon$.

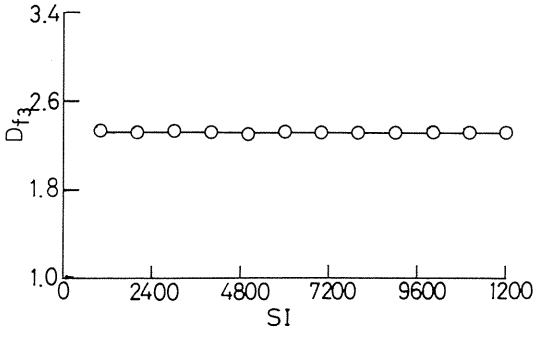

Fig. 4.4 Effect of the data segment length on the fractal dimension.

segment. When the value of SI is multiplied by the sampling time 0.2 msec, we obtain the real time length of the data segment.

4. 4 Results and discussions

Figures 4.5 (a) ~ 4.5 (f) show the curves of $\ln N(\varepsilon)$ vs. $\ln \varepsilon$ for the set of iso-concentration computed by the box-counting method at various x locations on the forward stagnation line of the sphere. At each x location, the change of curves of $\ln N(\varepsilon)$ vs. $\ln \varepsilon$ for various threshold level has been investigated. In these figures, L_Γ denotes the integral scale of the concentration field, and D_{f3} is the fractal dimension calculated from D_{f1} by Eq. (4.5). The two upward arrows drawn upon the abscissa in the figures indicate the high cutoff (which corresponds to the integral length scale of the concentration field) and the low end (which

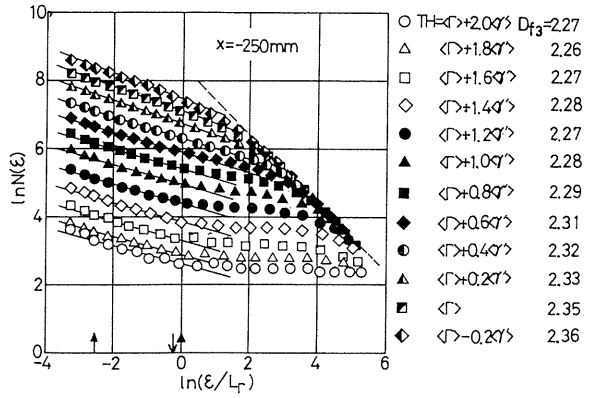

Fig. 4.5 (a) The curves of $\ln N(\varepsilon)$ vs. $\ln \varepsilon$ at $x = -250$ mm.

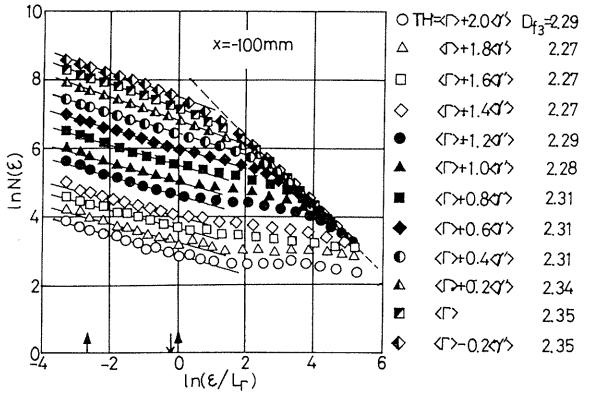

Fig. 4.5 (b) The curves of $\ln N(\varepsilon)$ vs. $\ln \varepsilon$ at $x = -100$ mm.

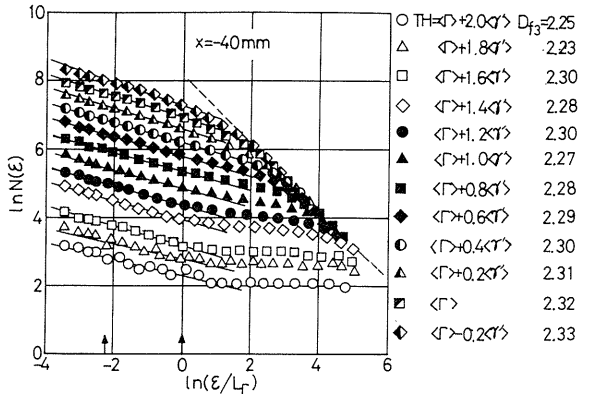

Fig. 4.5 (c) The curves of $\ln N(\varepsilon)$ vs. $\ln \varepsilon$ at $x = -40$ mm.

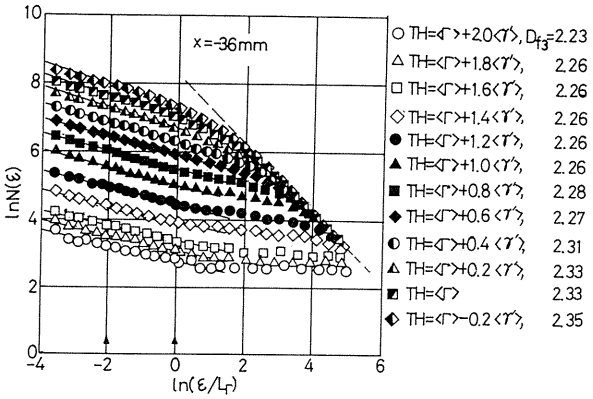

Fig. 4.5 (d) The curves of $\ln N(\varepsilon)$ vs. $\ln \varepsilon$ at $x = -36$ mm.

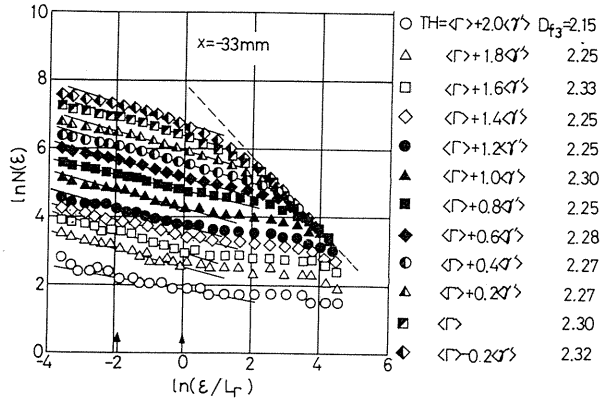

Fig. 4.5 (e) The curves of $\ln N(\varepsilon)$ vs. $\ln \varepsilon$ at $x = -33$ mm.

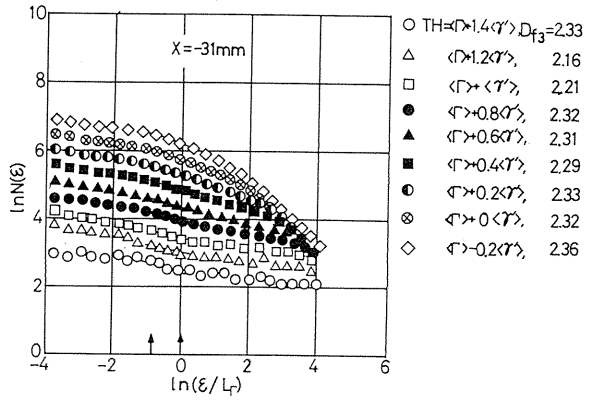

Fig. 4.5 (f) The curves of $\ln N(\varepsilon)$ vs. $\ln \varepsilon$ at $x = -31$ mm.

corresponds to the diameter of the laser beam) of the constant slope region in the curve of $\ln N(\varepsilon)$ vs. $\ln \varepsilon$. When the threshold TH is very large ($TH > \langle\Gamma\rangle + 2\langle\gamma'\rangle$), the number of iso-concentration points in the segment becomes too small to decide the value of D_{f3}. So we omitted the analysis of these cases of very large threshold. However, we can suppose[4-6] that the fractal dimension goes down as the threshold increases over $\langle\Gamma\rangle + 2\langle\gamma'\rangle$). On the other hand, it was also ascertained that as the threshold TH becomes smaller than $\langle\Gamma\rangle - 0.2\langle\gamma'\rangle$ the constant slope region of the curve of $\ln N(\varepsilon)$ vs. $\ln \varepsilon$ reduces gradually and vanish. Here it is noted that in the present experiments[4-1] on the stagnation line at the region far from the sphere, the intermittency factor $I_\Gamma \sim 0.75$ and $\langle\gamma'\rangle/\langle\Gamma\rangle \sim 1.2$, so we can estimate the value of $\langle\Gamma\rangle - 0.2\langle\gamma'\rangle$ as $\langle\Gamma\rangle - 0.2\langle\gamma'\rangle \sim 0.76\langle\Gamma\rangle = 0.76\Gamma/I_\Gamma = \Gamma$. In considering the above estimation, we find that the present results under the threshold of $\langle\Gamma\rangle - 0.2\langle\gamma'\rangle$ are not contradictory to other report by Sreenivasan & Meneveau[4-4], where they found that the fractality of the iso-concentration surface of the passive scalar in the turbulent jet vanishes around at the threshold of the mean concentration Γ.

From Figs. 4.5 (a) ~ (f), as the whole tendency it is found that when the threshold TH is larger than $\langle\Gamma\rangle + 1.2\langle\gamma'\rangle$, the curve of $\ln N(\varepsilon)$ vs. $\ln \varepsilon$ shows a good linear relation at the ε-region less than the integral scale L_Γ, but deviates from the straight line at the ε-region larger than L_Γ. In sections 3.4 and 4.2, it was shown that at $x = -250$ mm ~ -90 mm, L_Γ is about 2.0 mm and η is about 1.0 mm. In Figs. 4.5 (a) and (b), the downward arrow indicates the position of ε corresponding to the Kolmogorov scale η. Since the difference between η and L_Γ is small, the above results show that the fractality only in the small part of the K-range (between η and the integral length scale L (about 10 mm) for the velocity fluctuation) could be caught in the case of the large threshold. However, in the most range of the threshold ($\langle\Gamma\rangle + 0.4\langle\gamma'\rangle \leq TH < \langle\Gamma\rangle = 1.2\langle\gamma'\rangle$), we can observe that the constant slope region extends to the larger size of ε. From this result, the fractality in the wider part of the K-range can be recognized.

The dependency of the fractal dimension on the threshold at the various x positions on the stagnation line has been examined, and its result is shown in Fig. 4.6. From Fig. 4.6 and the values of D_{f3} given in the right hand side of Figs. 4.5 (a) ~ (f), it is found that, for the threshold between $\langle\Gamma\rangle - 0.2\langle\gamma'\rangle$ and $\langle\Gamma\rangle + 2.0\langle\gamma'\rangle$, the fractal dimensions do not almost change, and their magnitudes show the constant value of about 0.3.

Figure 4.7 shows the change of the fractal dimension as approaching to the sphere on the stagnation line. The fractal dimension keeps the almost constant value, so we conclude that the distortion of the flow due to the sphere in this experiment has almost no effect on the magnitude of the fractal dimension. Next, we will discuss about the above result. Now, we consider the fractal set of points (for simplicity, the set of points embedded in one-dimensional space), which dimension (box-dimension) is D_{f1}. So by applying the box-counting method for this set of points, the following equation holds

$$N(\varepsilon) \sim \varepsilon^{-D_{f1}}. \tag{4.7}$$

Here we assume that this fractal set receives the uniform distortion of compression so that the initial size of box ε reduces to ε' as the new size of box for this compressed set of points and apply the box counting method again, we naturally obtain

$$N(\varepsilon') = N(\varepsilon) \sim \varepsilon^{-D_{f1}}. \tag{4.8}$$

This is because the number of box covering the set of points does not change by the uniform

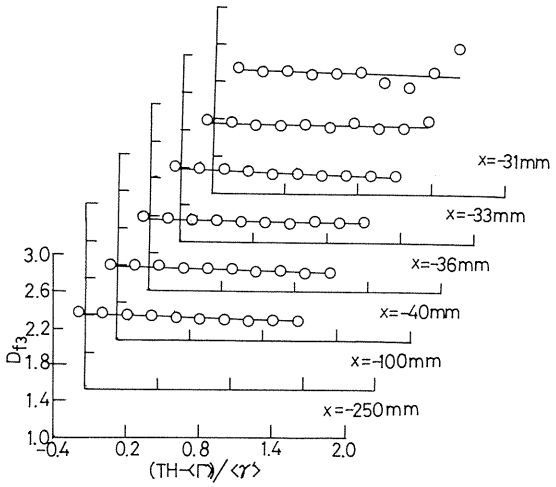

Fig. 4.6 Dependency of fractal dimension on the threshold value.

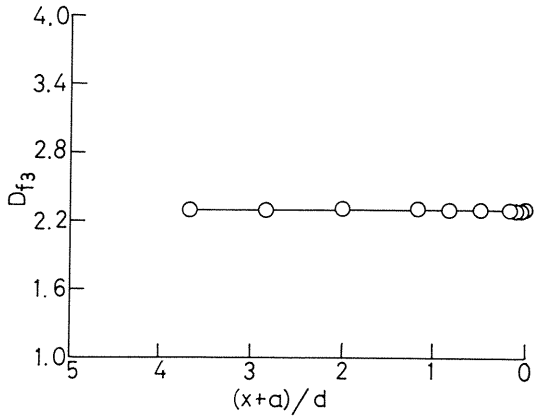

Fig. 4.7 Variation of fractal dimension on the stagnation line.

distortion. Let $\alpha = \varepsilon'/\varepsilon$. then the Eq. (4.8) can be expressed as

$$N(\varepsilon') \sim \varepsilon^{-D_{f1}} = \varepsilon'^{-D_{f1}} \alpha^{-D_{f1}} \varepsilon'^{-D_{f1}}, \tag{4.9}$$

where the parameter α is the real number which represents the magnitude of distortion. The Eq. (4.9) means that the uniform distortion does not influence the fractal dimension of the set of points on the one-dimensional line. On the other hand, in the case of the non-uniform distortion, the situation is different from the uniform case. Next, we will consider the effect of the non-uniform distortion. Since it is very difficult to deal with the effect of the non-uniform distortion in a strict sense of mathematics, here we will make some modelling of the

non-uniform distortion. We supose that the original set of points can be divided into n subsets, and each subset receives the uniform distortion locally, but the distortion parameter α is different between each subset. By applying the box-counting method again for these subsets, the same type of equation as the uniform distortion case holds also for the i-th subset,

$$N_i(\varepsilon') \sim \varepsilon^{-D_{f1}}, \tag{4.10}$$

where ε and ε' are respectively the size of box before and after the distortion, and N_i is the number of box to cover the i-th subset of points. Here we introduce the proportion constant a_i for the Eq. (4.10). Then we obtain

$$N_i(\varepsilon') = a_i \varepsilon^{-D_{f1}}. \tag{4.11}$$

It should be noted that the proportion constant a_i is different between each subset of points. On the other hand, by applying the box-counting method to the whole set of points, it is easily found that the number of box with size ε needed to cover the whole set is the sum of $N_i(\varepsilon)$. This leads to

$$\begin{aligned} N(\varepsilon) &= \sum_{i=1}^{n} N_i(\varepsilon) = \sum_{i=1} a_i \varepsilon^{-D_{f1}} \\ &= \left(\sum_{i=1}^{n} a_i \right) \varepsilon^{-D_{f1}}. \end{aligned} \tag{4.12}$$

The above equation means that even in the case of non-uniform distortion the fractal dimension (box-dimension) does not change from the set before the distortion to one after the distortion. It should be here noticed that, for the actual physical sets which can be regarded as fractal sets, the scaling law of $N_i(\varepsilon') \sim \varepsilon^{-D_{f1}}$ *holds only in the finite region of* ε *i.e.* $\varepsilon_{min} \leq \varepsilon \leq \varepsilon_{max}$. And this region of ε is expected to change due to the distortion. Here we assume that this region of ε for each subset becomes $b_i = [\varepsilon_{i,min}, \varepsilon_{i,max}]$ after the distortion. In order to find the fractality in some region of ε for the whole set, it is necessary that the following equation holds

$$b = \bigcap_i b_i \neq 0, \tag{4.13}$$

where the symbol $\bigcap_i b_i$ denotes the intersection of b_i. Therefore, there is the possibility that the non-uniformity of the distortion is too large for the above equation to hold so that the fractality can not be observed. However, even in this case we naturally expect that the fractality still exit locally. Next, we will see the results of the spatial region where the fractal structure can be observed. From Figs. 4.5(a) and 4.5(b), it is clearly found that there is a big difference on the spatial region of fractality between at $x = -250$ mm and $x = -31$ mm (the spatial region of the fractality at $x = -31$ mm is ten times smaller than one at $x = -250$ mm).

The fractal dimension D_{f3} for the iso-concentration surface is found to be about 2.3 in this work and this value agrees well with the result $D_{f3} = 2.36 \pm 0.05$ reported by Sreenivasan et. al.[4-5]. It must be noted here that the $\ln N(\varepsilon) \sim \ln \varepsilon$ distributions in Fig. 4.5 have a linearity which corresponds to the fractal dimension 2.3 even in a smaller scale region than the Kolmogorov time scale. This value 2.3 is smaller than the B-range fractal dimension

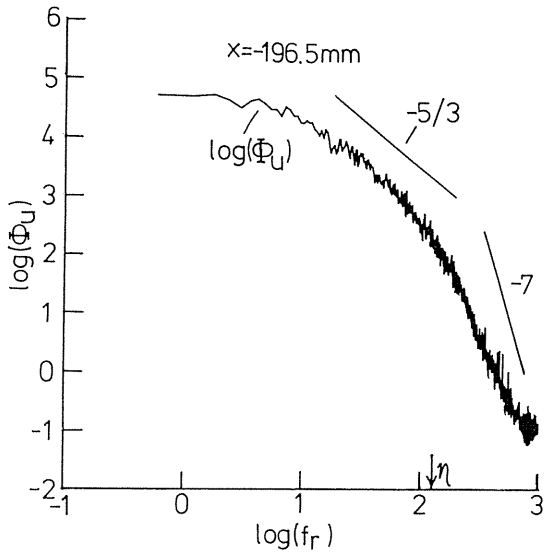

Fig. 4.8 Distribution of the velocity spectrum.

$D_{f3} \simeq 2.75$ which has been suggested by Prasad & Sreenivasan[4-5] and Sreenivasan & Meneveau[4-4]. This disagreement between our value and theirs may be possibly due to the finite spatial resolution of our concentration measuring probe. Prasad & Sreenivasan[4-8] showed experimentally that the fractal dimension in the B-range depends on the thickness of the laser sheet in their LIF measurement (note that the sheet thickness corresponds to the sampling length L_p in our measuring probe). If we accept the result by Prasad & Sreenivasan, it is not expected that the fractal dimension in the B-range could be obtained by the probe whose sampling length L_p is shorter than η but longer than η_B. Since our sampling length L_p (about 0.31 mm) is longer than η_B (about 0.016 mm), this effect of L_p would be one of the reasons of the disagreement[4-5),4-8]. We also consider, as mentioned in the §4.2, that the measured structure of the iso-concentration surface has less complexity than the original one because it is the result of the superposition of the many sectional structures[4-8] in the sampling volume. However, these conjectures have no mathematical fundamentals and thus we will need a further consideration.

Our another interesting result is that the concentration field can have a fractal feature, even though there exists no clear inertial sub-range (the $-5/3$ power range) in the spectrum distributions for the velocity and concentration fluctuations. Fig. 4.8 shows the velocity spectrum distribution measured at $x = -196.5$ mm. No appreciable region of the $-5/3$ power law can be found from the figure. We have reported that the inertial sub-range could not be seen also in the concentration fluctuation spectrum[4-2]. In spite of these facts, however, the fractal structure does exist certainly in the set of the iso-concentration points as shown in Fig. 4.5. We infer this reason as follows. The fractal structure in the diffusion field could be formed more efficiently by the non-linear Lagrangian relative motion of fluid particles[4-13] (the cascade process through stretching and folding, see figure 4.9), rather than by the self-similarity in the velocity field (the inertial subrange). Therefore, this non-linear particle motion would be a source of the observed fractal feature of the iso-concentration points set,

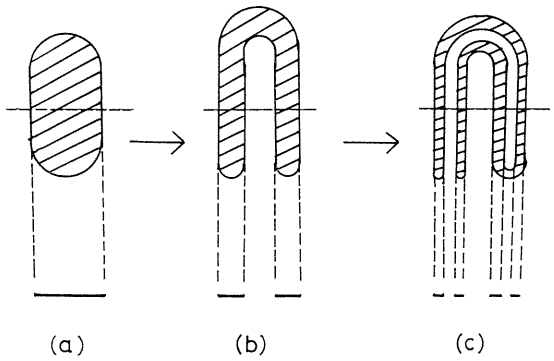

Fig. 4.9 Cascade model by the stretching and folding.

because the non-linearity causes the diffusion structure of plume to be chaotic. It is concluded from the above argument that the fractal feature in the concentration field can exist even though there does not exist a clear region of the $-5/3$ power law in the velocity spectrum.

It is also interesting to note that the concentration field has a fractal feature even in the case that its spectrum does not have the region of the $-5/3$ power law. Recently, assuming that the concentration signal is approximated by a series of rectangular pulses, Hunt & Vassilicos[4-11] showed the following relation between the fractal dimension D_{f2} of the material surface in the diffusion field (consider the case of two dimensional surface) and the slope β of a linear part in its concentration spectrum[4-11),4-12],

$$D_{f2} = 3 + \beta. \tag{4.14}$$

If we apply their theory to our result, $\beta \simeq -1.7 \simeq -5/3$ can be obtained readily from $D_{f2} = D_{f3} - 1 \simeq 1.3$. However, it is not expected that the above relation would be appropriate to our case, because Fig. 4.2 shows clearly that our concentration signal is completely different from a rectangular series. In order to check their theory, we analyzed the concentration signal which was digitalized by the following equation with a threshold level TH,

$$\tilde{\Gamma}' = \begin{cases} 1 & \text{if } \tilde{\Gamma} > TH \\ 0 & \text{otherwise} \end{cases} . \tag{4.15}$$

The resultant spectrum for $\tilde{\Gamma}'$ is shown in Fig. 4.10. It is found from the figure that this spectrum has a clear linear part over a wide wave-number range and its slope is nearly $-5/3$.

Now, we describe a simple modeling for the cascade process of the diffusion field shown in Fig. 4.9. It is assumed in this model that the cascade process consists of only the stretching and the folding of the material lump. As shown in Fig. 4.9, the material lump is stretched by the turbulence distortion until its length surpasses the turbulence integral scale, and then the folding process of the lump by the turbulence eddy starts. After a series of such processes is repeated again and again, a complex convoluted diffusion structure (a filament or a striation

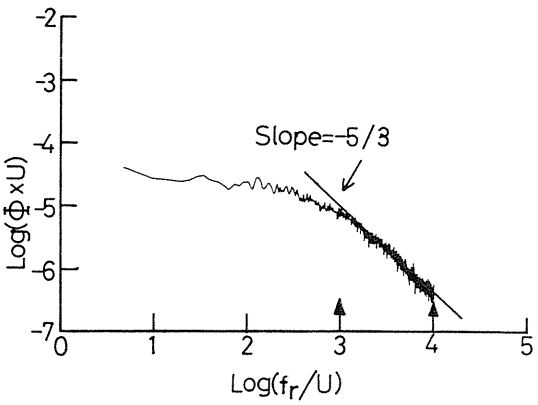

Fig. 4.10 Spectrum of the digitalized concentration signal.

structure[4-1),4-13)]) will be formed finally. Since such formation of the diffusion structure always involves the entrainment of the ambient fluid, the mixing rate of the diffusing matter in the structure would become smaller and smaller as the process proceeds. The set of points obtained from the one-dimensional intersection of this structure with a straight line is very similar with the Cantor set. In fact, the fractal dimension of the 1-scale Cantor set with a scale factor 1/8 is

$$D_f = -\log 2/\log(1/8) = 0.333, \tag{4.16}$$

and this value is found to be almost the same with the fractal dimension of the set of the iso-concentration points obtained from our analysis.

4. 5 Conclusions

(1) The set of the iso-concentration points can have a fractal feature, even though there exists no range of the $-5/3$ power law in the distributions of the velocity and concentration spectra. This fractal dimension D_{f1} was found to be about 0.3, independently of the threshold level, and this value agreed well with the K-range fractal dimension which have been obtained in high Reynolds number turbulent flows[4-3),4-8)].

(2) The fractal dimension of the set of the iso-concentration points was shown to keep a nearly constant value on the front stagnation line. This can be explained by assuming a uniform or a partially uniform distortion of the material lump.

References of chapter 4

4-1) Liu, S., Tsunoda, H., Sakai, Y. & Nakamura, I., "Stochastic characteristics of a point-source plume diffusion field upstream of a sphere", *Trans. JSME.*, Vol.57, No.541 (1991), 2976, (in Japanese).

4-2) Sakai, Y., Liu, S., Tsunoda, H., & Nakamura, I., "On the Statistics of a point-source plume around the sphere", *Trans. JSME,* Vol.58, No.545 (1992), 51, (in Japanese).
4-3) Mandelbrot, B. B., *The Fractal Geometry of Nature,* Freeman (1982), San Francisco.
4-4) Sreenivasan, K.R. & Meneveau, C., "The fractal facets of turbulence", *J. Fluid Mech.,* Vol.173 (1986), 357.
4-5) Sreenivasan, K.R., "Fractals and multifractals in fluid turbulence", *Ann. Rev. Fluid Mech.,* Vol.23 (1991), 539.
4-6) Sreenivasan, K.R., Ramshankar, R. & Meneveau, C., "Mixing, entrainment and fractal dimension of surface in turbulent flow", *Proc. R. Soc. Lond.,* A421 (1989), 79.
4-7) Tennekes, H. & Lumley, J. L., *A First Course in Turbulence,* The MIT Press (1973), 72.
4-8) Prasad, R.R. & Sreenivasan, K.R., "The measurement and interpretation of fractal dimensions of surfaces in turbulent flows", *Phys. Fluids,* Vol.A2, No.5 (1990), 792.
4-9) Takayasu, H., *Fractal,* Asakura Press (1986), Tokyo, (in Japanese).
4-10) Feder, J., *Fractals* (1988), Plenum Press, 12.
4-11) Hunt, J.C.R. & Vassilicos, J.C., "Kolmogorov's contributions to the physical geometric university", *Proc. R. Soc. Lond.,* Vol.A434 (1991), 183.
4-12) Vassilicos, J.C. & Hunt, J.C.R., "Fractal dimensions and spectra of interfaces with application to turbulence", *Proc. R. Soc. Lond.,* Vol.A435 (1991), 505.
4-13) Ottino, J.M., *The Kinematics of Mixing: Stretching, Chaos and Transport,* Cambridge University Press (1989), 1.

Acknowledgments

The authors are grateful to Mr. Takehiro KUSHIDA and Mr. Hatsuo MURAKAMI at the department of Mechanical Engineering of Nagoya University for their technical assistances. We are also indebted to the fruitful discussions on the fractal analysis with Dr. J.C. Vassilicos at University of Cambridge in U.K. and Dr. Y. Tsuji at the Department of Nuclear Engineering of Nagoya University. Further, we wish to express sincere thanks to Prof. J.C.R. Hunt at Meteorological Office in U.K. for invaluable advices and suggestions on turbulent diffusion phenomena. A part of this work was supported by the Japan Ministry of Education under Grant No.02402026.